Landscape and Urban Planning 264 (2025) 105490

Contents lists available at ScienceDirect

Landscape and Urban Planning

journal homepage: www.elsevier.com/locate/landurbplan

Optimizing urban three-dimensional landscapes in potential development areas to mitigate urban heat island effect under shared socioeconomic pathways

Shiyu Xiao [a,1], Jialyu He [b,c,d,1], Yao Yao [a,e,f], Xun Liang [a,g], Xia Li [h,*]

[a] UrbanComp Lab, School of Geography and Information Engineering, China University of Geosciences, Wuhan, Hubei 430078, PR China
[b] The Third Surveying and Mapping Institute of Hunan Province, Changsha 410000, PR China
[c] Hunan Geospatial Information Engineering and Technology Research Center, Changsha 410000, PR China
[d] Hunan Engineering Research Center of Geographic Information Security and Application, Changsha 410000, PR China
[e] LocationMind Institution, LocationMind Inc., Chiyoda, Tokyo 101-0048, Japan
[f] Hitotsubashi Institute for Advanced Study, Hitotsubashi University, Kunitachi, Tokyo 186-8601, Japan
[g] National Engineering Research Center of GIS, China University of Geosciences, Wuhan, Hubei 430078, PR China
[h] Key Laboratory of Geographic Information Science (Ministry of Education), School of Geographic Sciences, East China Normal University, Shanghai 200241, PR China

HIGHLIGHTS

- Urban three-dimensional landscapes were incorporated during the optimization process.
- Performance of optimization was enhanced due to potential development areas.
- Future land use spatial structure was optimized under shared socioeconomic pathways.
- Decline in heatstroke incidents was projected based on the optimization results.

ARTICLE INFO

Keywords:
Land use spatial structure optimization
Urban heat island
Urban three-dimensional landscape
Potential development areas
Shared socioeconomic pathways

ABSTRACT

The urban heat island (UHI) effect threatens human health. While optimizing the spatial structure of urban land use presents a promising strategy for UHI mitigation, few studies examined the feasibility of urban three-dimensional landscape optimization in potential development areas (PDA), resulting in unsuitable optimization results and computational inefficiency. To address these limitations, we develop a novel multi-objective optimization model for urban three-dimensional landscapes in PDA (3DLS-PO) that integrates the patch-generating simulation (PLUS) model and the particle swarm optimization (PSO) algorithm. The PLUS model first simulates the PDA in the future under different scenarios. The PSO algorithm then allocates urban land use in the PDA to mitigate the UHI effects with the explored nonlinear relationship between land surface temperature (LST) and urban two- and three-dimensional landscapes. We applied the 3DLS-PO model to the Tokyo Metropolitan Area (TMA) for 2030 under the shared socioeconomic pathway (SSP) scenarios. The SSP5 scenario achieves the maximum LST reduction of 5.18%, followed by SSP1 (4.60%) and SSP2 (2.34%). To mitigate the UHI effects in the TMA, high-rise buildings should be placed at the periphery of the TMA, low-rise buildings should be allocated to the suburbs, and green spaces should be scattered. The optimization results demonstrate substantial public health benefits, potentially preventing 3.01%-14.10% of heatstroke incidents in Tokyo. Incorporating the PDA also enhances the computational efficiency of the optimization process by 14 times. The 3DLS-PO model can provide support for addressing urban climate change.

* Corresponding author.
E-mail address: lixia@geo.ecnu.edu.cn (X. Li).
[1] These authors contributed equally: Shiyu Xiao, Jialyu He.

https://doi.org/10.1016/j.landurbplan.2025.105490
Received 21 February 2025; Received in revised form 14 July 2025; Accepted 4 September 2025

1. Introduction

Urban heat island (UHI) is a phenomenon where the temperature in urban areas is higher than that in rural areas (Varentsova & Varentsov, 2021). With global warming, the threat posed by UHI to human health is becoming increasingly severe (Akkose et al., 2021; Santamouris, 2020). The causes of the UHI effect are very complex. Climate change exacerbates urban thermal environment problems by increasing temperatures, altering precipitation patterns, and intensifying extreme weather events. Human activities have directly or indirectly altered the urban thermal environment by releasing anthropogenic heat and modifying the surface structure, and are a significant driving factor for the increase in the UHI index on a large scale (Peng et al., 2025; Yang et al., 2025). Hard surfaces (asphalt, concrete) can reduce bioclimatic comfort by approximately 20 % and are the primary source of the UHI effect (Zhang et al., 2024). In the future, under various scenarios (such as SSP1 and SSP5), if effective adaptation strategies are lacking, the average urban temperature is expected to rise significantly, and the UHI effect is likely to intensify substantially (Wang et al., 2025). Therefore, it has become increasingly important to forecast future UHI effects under different socioeconomic scenarios and to formulate appropriate prevention measures.

Urban areas are composed of different types of land use and land cover (Vanderhaegen & Canters, 2017), such as residential, commercial, and industrial lands, each with different thermal characteristics (Wu, 2014; Zhou et al., 2017). The quantity and spatial structure of these areas significantly influence the intensity of UHI effects (Li & Zhou, 2019). Hu et al. (2024) noted that the reduction of farmland and forest areas, as well as the expansion of impervious surfaces (such as buildings and roads), are significant factors contributing to the increase in urban thermal discomfort. On the contrary, greenland and water bodies within cities can provide cooling effects (Tan et al., 2021). Specifically, larger greenland provides higher cooling effects, and circular or square greenlands significantly correlate with LST (Yu et al., 2017). In contrast, factory and residential areas tend to exacerbate the UHI effects. For instance, the distance to industrial land could explain 26 % of temperature variations at 4 PM (Coseo & Larsen, 2014). The increasing demand for residential areas brought by rapid urbanization has also promoted the UHI effect in cities (Zhao et al., 2022).

In addition to the above two-dimensional spatial structures of land use, the urban three-dimensional landscape plays a crucial role in shaping UHI effects (Yu et al., 2021). Buildings, as key components of the urban three-dimensional landscape, influence the UHI effects by altering the reflection and absorption of solar radiation as well as heat dispersion (Futcher et al., 2017). Specifically, LST correlates significantly with both two- and three-dimensional urban landscapes (Huang & Wang, 2019). High-rise buildings might mitigate UHI intensity at pedestrian levels due to their shading effects (Zhou & Chen, 2018). The average urban albedo decreases with the increase of building height, and the greater the height difference of buildings, the greater the solar radiation absorbed (Yang & Li, 2015). Urban three-dimensional landscapes correlate more strongly with local thermal comfort than that at the two-dimensional level (Zhang et al., 2022). The above studies explored the impacts of urban two- or three-dimensional landscapes on the UHI effect. Based on this relationship, optimizing the spatial structures of land use can contribute to mitigating the UHI effects for assisting urban planning (Qiu et al., 2023). However, previous studies only optimized the spatial structure of land use from a two-dimensional perspective (Ahmed et al., 2024; Qiu et al., 2023; Wardeh et al., 2022). Considering mega-cities often feature a mix of high- and low-rise buildings (Zhang et al., 2020), the spatial morphology and surface roughness of the built environment assessed at the three-dimensional level exhibit more significant spatial heterogeneity. Therefore, mitigating the UHI effect by optimizing the urban three-dimensional landscapes would be more comprehensive.

There has been a lot of research in the field of land use spatial structure optimization (Rahman & Szabó, 2021). While few researchers have only one objective in optimizing the spatial structure of land use, multi-objective spatial optimization has emerged as the mainstream research direction (N. Wang et al., 2024; Pan et al., 2023; Song & Chen, 2018). Typical methods for optimizing the spatial structures of land use under multiple future scenarios generally involve calculating land use demands for each scenario and then randomly rearranging all land parcels within the study area before optimization (Tong, Yang, et al., 2024). However, these methods started optimization from randomly shuffled land parcels and ignored the historical information of land use change (Tong, Liu, et al., 2024). As a result, some optimized land parcels might have a low likelihood of conversion, exhibiting unsuitable land use spatial structure (Pan et al., 2021). Furthermore, since the optimization is performed across the entire study area, the computational efficiency of the optimization process tends to be comparatively low, leading to excessive time consumption (Li et al., 2022). An efficient optimization strategy worth exploring is first identifying the land parcels with conversion potential and then optimizing the spatial structure of land use. During land use change simulation, the potential development area (PDA) can reflect the likelihood of future conversion for each land parcel (Chen et al., 2020; Verburg et al., 2013). Therefore, it is feasible to incorporate PDA into the optimization framework to enhance its practicability.

Inspired by the facts, this study proposes a novel multi-objective optimization model for urban three-dimensional landscapes within PDA (3DLS-PO) that performs spatial optimization under the shared socioeconomic pathway (SSP) scenarios. The patch-generating simulation (PLUS) model (Liang et al., 2021) and the particle swarm optimization (PSO) algorithm (Kennedy & Eberhart, 1995) consist of this proposed 3DLS-PO model. We used the PLUS model to simulate PDA, then the UHI effects in the TMA were optimized using the PSO algorithm. This study selects the Tokyo Metropolitan Area (TMA) under SSP scenarios as the study area. TMA is located in a humid subtropical region with complex land use patterns, experiencing severe heatwaves from May to October. Compared to 2000, Tokyo's population growth rate reached 16 % in 2020, with a population of 14 million and a population density of 7866 people per km2. As the political, economic, and cultural center of Japan, TMA's large population and urban infrastructure development have contributed to urban warming and exacerbated a climate crisis. The severe UHI effect poses a threat to people's health. Therefore, mitigating the UHI effect is one of the prominent challenges for TMA. Land surface temperature (LST) retrieved from Landsat images is a critical index to quantitatively describe the relationship between land use and the UHI effects (Tanoori et al., 2024). We optimized the spatial pattern of TMA with multiple goals of minimizing LST and maximizing urban development suitability. SSPs contain multiple narratives on the future development trends of the economy and society (O'Neill et al., 2014), which can provide multiple future urban development scenarios for this study. The optimization results can indicate the changes in LST, average building height, and spatial structure of land use between initial and optimized state, thus assisting urban planning under SSPs.

2. Materials

2.1. Study area and data sources

This study focuses on TMA as the study area. TMA covers approximately 13,500 km^2 and comprises four primary administrative divisions: Tokyo, Kanagawa, Chiba and Saitama. Currently, TMA is adversely affected by UHI phenomena (O'Malley & Kikumoto, 2022), which coupled with an aging population and increasing incidence of heat-related illnesses (Kikumoto et al., 2016), poses a growing threat to public health.

Table 1 presents the data and their sources utilized in this study. Land use data from 2009 and 2021 are used to construct the PLUS

Table 1
Data required in this study.

Data	Format	Source
Road networks	Vector	Open Street Map (https://www.openstreetmap.org/)
Land use (2009 & 2021)	Raster (100 m)	The Ministry of Land, Infrastructure, Transport and Tourism of Japan (https://nlftp.mlit.go.jp/ksj/index.html)
DEM	Raster (250 m)	
POI	Vector	
Land price	Vector	
Population density	Raster (1000 m)	
SSP population	Raster (1000 m)	NASA SEDAC (https://sedac.ciesin.columbia.edu/)
LST	Raster (30 m)	The United States Geological Survey (https://earthexplorer.usgs.gov/)
Building footprint	Vector	3D-GloBFP (Che et al., 2024)

model. The road network, Digital Elevation Model (DEM), Points of Interest (POI), land price, and population density are used to extract the conversion rules of land parcels. SSP population raster data is utilized to estimate future land use demands. LST and building footprint data are used to establish the nonlinear relationships between land use structure, urban three-dimensional landscape, and LST.

2.2. Land use data

We downloaded the land use data with 100-meters spatial resolution for 2009 and 2021 from the Ministry of Land, Infrastructure, Transport and Tourism of Japan to simulate the land use change. This land use data is classified from satellite images based on electronic maps and topographic maps (https://nlftp.mlit.go.jp/ksj/index.html), which have high accuracy and authority. The land use data has already been applied in the land use simulation research (Du et al., 2018).

Local Climate Zone (LCZ) (Stewart & Oke, 2012) is a classification system used to describe types of urban and natural land surfaces, providing a standardized classification system for thermal environment research (R. Wang et al., 2024). Therefore, referring to the definition of LCZ, this study reclassifies the original land use data into the following 10 types (Table A1): farmland, forest, wasteland, high-rise building, factory, low-rise building, low-rise dense building, transportation, public service, and waterbody. Fig. 1 illustrates the spatial distribution of land use.

Tables 2 and 3 present the land use areas and transition matrix for 2009 and 2021. Between 2009 and 2021, significant changes in land use types occurred in the TMA, characterized mainly by a reduction in farmland, alongside an increase in high-rise buildings and transportation. Approximately 14.69 % of the land changed during this period. The main decrease in land use was observed in farmland, which was primarily converted into low-rise buildings.

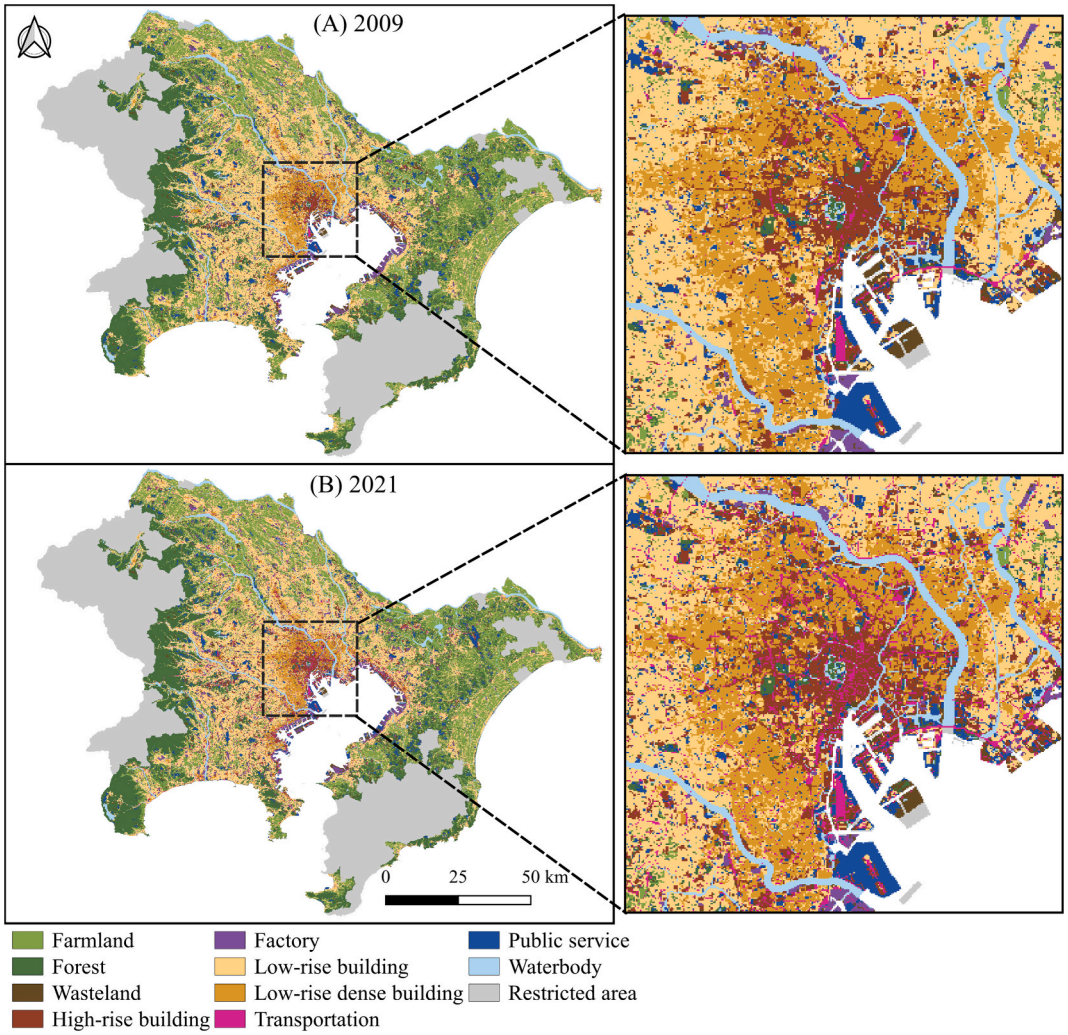

Fig. 1. Spatial distribution of land use in the TMA for 2009 and 2021.

Table 2
The area and rate of each land use type in the TMA in 2009 and 2021.

Type	2009		2021	
	Area (km^2)	Rate (%)	Area (km^2)	Rate (%)
Farmland	2535.45	27.21	2325.53	24.95
Forest	2000.62	21.48	1960.83	21.05
Wasteland	327.20	3.51	293.25	3.15
High-rise building	220.14	2.36	324.09	3.48
Factory	213.59	2.29	186.86	2.01
Low-rise building	3164.26	33.97	3148.34	33.80
Low-rise dense building	357.62	3.84	328.70	3.53
Transportation	53.61	0.58	244.54	2.63
Public service	443.01	4.76	503.36	5.40

2.3. Building footprint data

To model the relationship between land use and urban three-dimensional structure, it is necessary to use building footprint data that includes height attributes. The building footprint data utilized in this study is obtained from the 3D-GloBFP dataset (Che et al., 2024). In this dataset, each building is represented as a polygon feature with associated height attributes. Fig. A1 illustrates the building footprint data for the Shinjuku ward of Tokyo.

2.4. Land surface temperature data

We downloaded Landsat 8 Collection 2 Level-2 Science Products data on July 27, 2023, from the USGS (https://earthexplorer.usgs.gov/) to retrieve LST. This specific date was selected due to the least cloud cover over the TMA in recent years, ensuring reliable LST retrieval. Furthermore, records from the Japan Meteorological Agency (https://www.jma.go.jp/jma/press/2403/22b/ccmr2023.html) indicate that the long-term summer air temperature trend in Tokyo (1927–2023) increased at a rate of 2.3 ℃ per century. This modest rate of temperature trend suggests minimal interannual temperature variations during recent summers. Therefore, we applied the linear transformation equation (1) to retrieve LST from the 2023 Landsat 8 data (Z. Wang et al., 2024).

$$LST(K) = 0.00341802 \times DN + 149 \quad (1)$$

where DN is the raw Digital Number (pixel value). Fig. A2 shows the retrieved LST for the TMA.

2.5. Spatial variables

Spatial variables play a crucial role in driving urban land use change. To accurately simulate the land use change, it is essential to incorporate spatial variables, as their quality directly influences the estimation of land use conversion probabilities (He, Liu, et al., 2023). In this study, we utilized 19 spatial variables (Fig. A3): natural elements (topography, water bodies), transportation infrastructure (highways, railways, airports), locational features (city center, government offices), production and living facilities (bus stops, hospitals, parks, etc.), and economic factors (land prices, population). In addition to land use change simulation, spatial variables also influence the three-dimensional landscapes and LST. We utilized a subset of these 19 spatial variables that exhibit minimal change during the optimization process (Fig. A4) to predict urban three-dimensional landscapes and LST. All spatial variables share the same spatial resolution as the urban land use data.

3. Method

As shown in Fig. 2, this study proposes the 3DLS-PO model that performs spatial optimization only for land parcels within PDA under the SSP scenarios. This model integrates urban three-dimensional landscape information during optimization to minimize LST and maximize suitability. The 3DLS-PO model proposed in this study consists of a 2030 potential development area prediction module under SSP scenarios based on the PLUS model and a UHI effect optimization module that couples urban three-dimensional landscapes using the particle swarm algorithm.

3.1. Land use demand forecast for the TMA in 2030 under SSP scenarios

As illustrated in Fig. 2, the PLUS model needs land use demand as an input to predict future spatial structures of land use. This study predicts the land use demand for 2030 using SSP population raster, demographic yearbooks, and land use data. SSP includes several narratives that describe potential future development trends of human society until 2100 (O'Neill et al., 2014).

Since the SSP population raster only provides national-level data, it is necessary to localize the SSP population raster for TMA (Chen et al., 2024), as shown in Fig. 3. For urban land use types (high-rise building, factory, low-rise building, low-rise dense building, transportation and public service), we first established a linear regression between actual population and SSP population. The resulting regression equation (Table A1) is then used to estimate the localized SSP population for 2030. The urban land use demand is calculated by multiplying the estimated population by the per capita land area. For non-urban land use types (farmland, forest and wasteland), the land use demand for 2030 under SSP scenarios is calculated using the equation (2):

$$A_{ssp,i} = A_{2021,i} - \left(\sum_i A_{2021,i} - \left(T - \sum_i A_{ssp,i}\right)\right) \times \frac{A_{2009,i} - A_{2021,i}}{\sum_i A_{2009,i} - A_{2021,i}} \quad (2)$$

where A represents the land use area; SSP represents the SSP scenarios for the 2030; i represents the non-urban land use types; T represents the total area.

Table 3
Change in land use area (km^2) in the TMA from 2009 to 2021.

2009	2021								
	FL	For	WL	HRB	Fac	LRB	LRDB	Trans	PS
FL	2155.21	68.72	31.92	2.26	3.29	227.50	0.06	29.20	17.29
For	70.92	1789.92	27.96	3.38	1.49	67.83	0.30	12.82	26.00
WL	10.44	26.99	178.01	9.74	6.50	46.79	0.19	14.67	33.87
HRB	0.13	1.21	3.71	176.71	0.56	10.91	4.80	18.35	3.76
Fac	1.25	0.99	13.38	3.17	168.12	9.66	0.29	5.84	10.89
LRB	83.65	37.09	29.57	103.09	5.79	2756.86	12.25	94.63	41.33
LRDB	0.04	0.24	0.25	15.53	0.15	12.67	308.83	17.12	2.79
Trans	1.01	0.99	0.83	1.06	0.24	2.18	0.35	46.63	0.32
PS	2.88	34.68	7.62	9.15	0.72	13.94	1.63	5.28	367.11

Note: FL (farmland); For (forest); WL (wasteland); HRB (high-rise building); Fac (factory); LRB (low-rise building); LRDB (low-rise dense building); Trans (transportation); PS (public service).

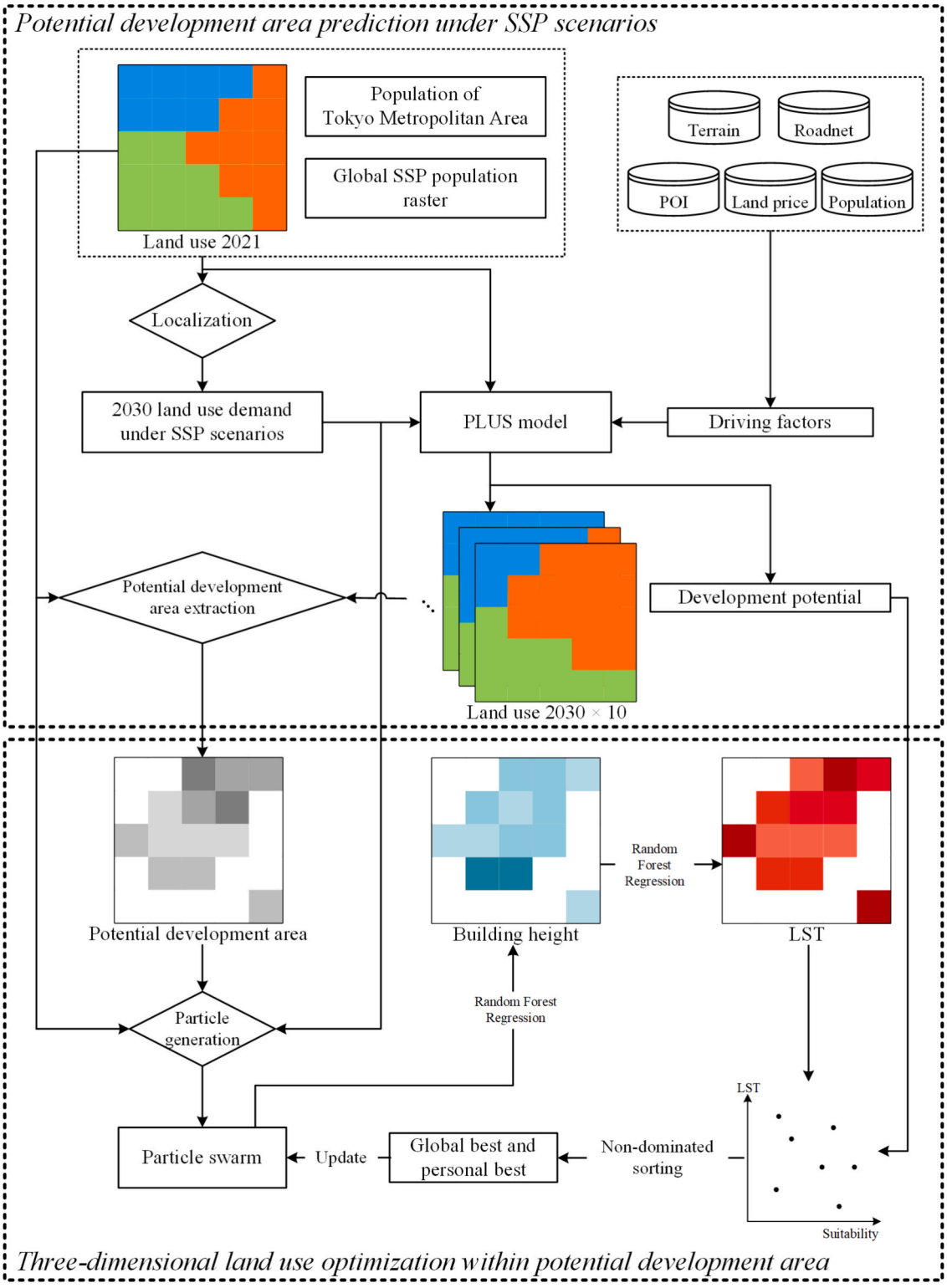

Fig. 2. Flowchart of the 3DLS-PO model.

3.2. *Potential development area prediction based on PLUS model*

This study employs the PLUS model (Liang et al., 2021) to forecast the spatial structures of land use of the TMA in 2030 under SSP scenarios. The inputs for the PLUS model include the land use demand for 2030, the 2021 land use map, and driving variables. The outputs of the PLUS model are the land use map for 2030 and a development potential map. Ten-year span was reasonable for validating the feasibility of land use simulation and optimization (M. Cao et al., 2022; Meimei et al., 2023).

The PLUS model comprises two main modules: the Land Expansion Analysis Strategy (LEAS) module and the CA based on multi-type Random path Seed (CARS) module. The LEAS module constructs a separate random forest model for each land use type to explore the transition rules for each land use type. The CARS module is a CA model that incorporates a multi-type patch generation mechanism, integrating

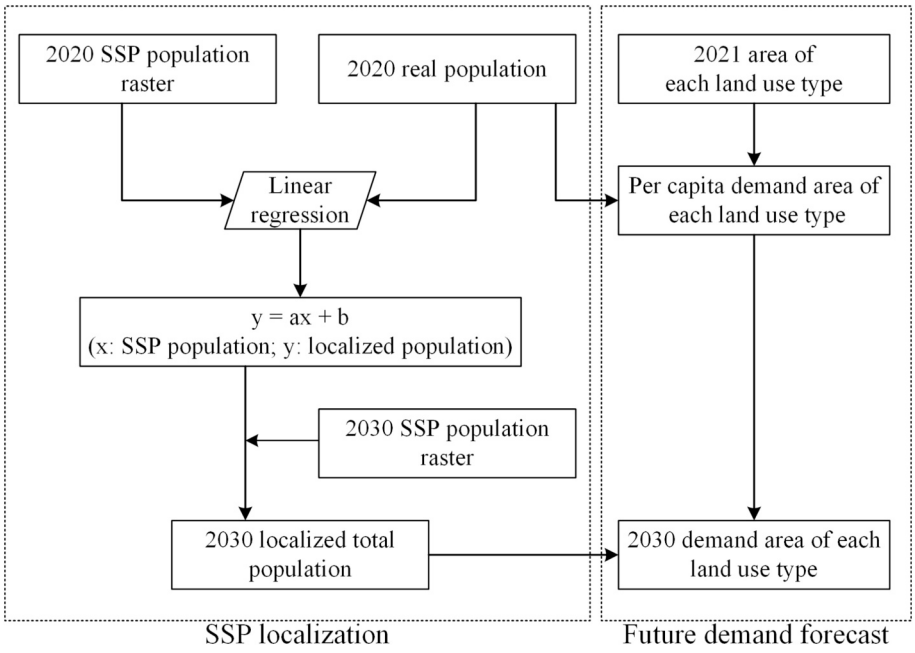

Fig. 3. Flowchart of the forecasting method for future urban land use demand under SSP scenarios.

both "top-down" (macroscopic overall land use demand) and "bottom-up" (local land use competition) mechanisms. During the simulation process, CARS influences the overall conversion probability by calculating adaptive inertia coefficients, thereby driving each type of land use to meet demand.

This study validates the PLUS model's performance using the Figure of Merit (FoM) accuracy metric, Overall Accuracy (OA), Kappa coefficient, and landscape metrics by comparing the ground truth and land use simulation in 2021. FoM is calculated as the ratio of correctly predicted changes to the total number of predicted changes, excluding unchanged cells from the correct predictions. It provides a relatively comprehensive evaluation of the model and is widely used in CA simulation studies (Chen et al., 2014; X. Li et al., 2020). OA represents the ratio of correctly simulated cells to the total number of cells and is widely used for model accuracy assessment (Han & Jia, 2017). The Kappa coefficient measures consistency and is similarly employed in the evaluation of CA simulation accuracy (Liu et al., 2017). The formulas for the FoM metric, OA metric, and Kappa coefficient are shown in equations (3), (4), and (5), respectively.

$$FoM = \frac{B}{A + B + C + D} \tag{3}$$

$$OA = 1 - \frac{A + C + D}{N} \tag{4}$$

$$Kappa = \frac{P_0 - P_e}{1 - P_e} \tag{5}$$

where A represents the number of land parcels that actually changed but were not simulated as changed; B represents the number of land parcels that actually changed and were correctly simulated as changed; C represents the number of land parcels that actually changed but were incorrectly simulated as changed; D represents the number of land parcels that did not actually change but were simulated as changed; N represents the total number of cells in the study area; P_0 represents the accuracy of the prediction; and P_e represents the chance agreement.

By inputting the land use demand, the 2021 land use map, and the spatial variables into the calibrated PLUS model, the land use map for 2030 was simulated. To identify the PDA, the simulation process was repeated 10 times. As shown in Fig. 4, each 2030 land use map was compared with the 2021 map to identify the change areas. These change maps were then summed pixel by pixel, and the result was divided by 10 to obtain the PDA. The pixel values in the PDA indicate the likelihood of land use change occurring between 2021 and 2030.

3.3. UHI effect mitigation using PSO within PDA

The optimization problem addressed by 3DLS-PO consists of two objective functions: minimizing LST and maximizing suitability (Fig. 5). To minimize LST during the optimization process, we need to mine the nonlinear relationship between LST and the spatial structure of land use. The mined nonlinear relationship was applied to predict LST after each step during the optimization process in PDA. Using the PSO algorithm, we can reallocate the spatial structure of land use to mitigate the UHI effect based on SSP scenarios. The following sections will provide a detailed explanation of multi-objective functions and technical details.

3.3.1. Multi-objective functions

(1) Minimizing LST

The optimization problem of the UHI effect in this study can be described as follows: for the land parcels within the PDA, reallocate their spatial positions and estimate the average height of the buildings within these land parcels, so that the spatial structure of land use optimally achieves the objective of minimizing the sum of LST for the land parcels in the PDA. Besides the three-dimensional landscape of buildings and the two-dimensional land use density within the neighborhood, we also considered spatial variables (Fig. A4) that exhibit minimal change during the optimization process as independent variables for fitting LST. The objective function for optimizing the UHI effect by coupling average building height is presented in equations (6) and (7):

$$Max \sum_{i=1}^{N} -f_{LST}(f_H(LUD_i, SV_i), LUD_i, SV_i) \tag{6}$$

$$LUD_i^k = \frac{\sum_{M \times M} con(c_i = k)}{M \times M} \tag{7}$$

where i represents the i-th parcel; N is the number of parcels in the PDA; LUD_i (Land Use Density) is the land use density of various land use types for the i-th parcel; SV_i (Spatial Variable) is the spatial variable for the i-th

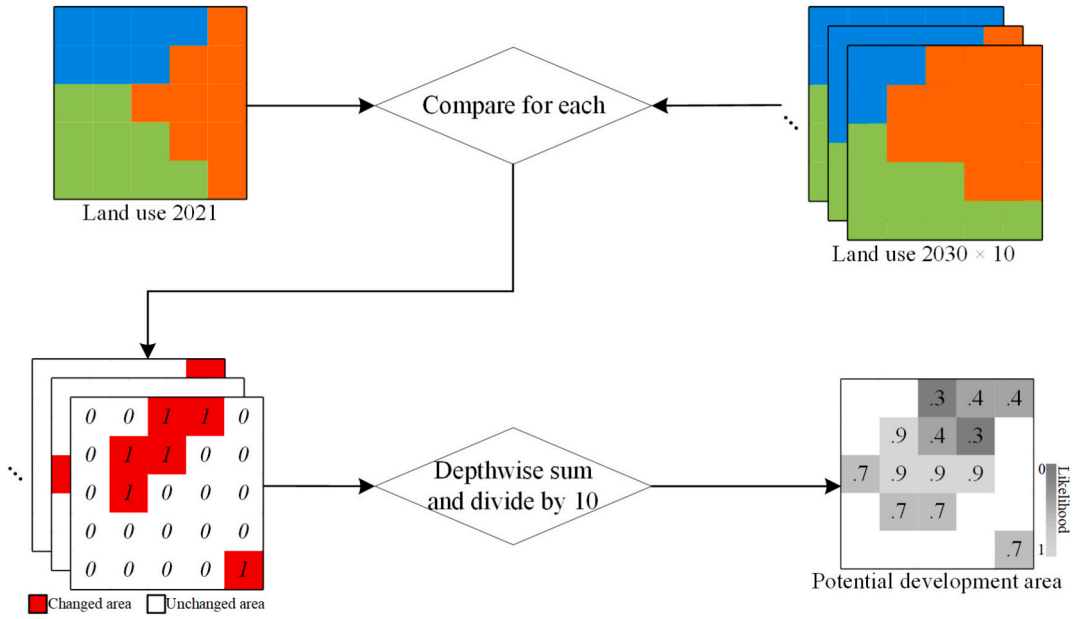

Fig. 4. Potential development area extraction.

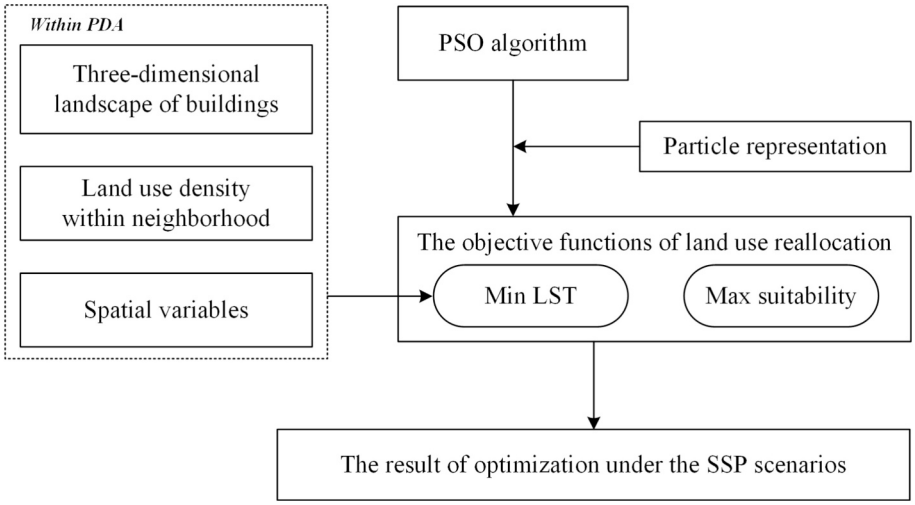

Fig. 5. Flowchart of UHI effect mitigation using PSO within PDA.

parcel; f_H is the function for estimating the average building height within parcels; f_{LST} is the function for estimating the LST within parcels; LUD_i^k represents the land use density of land use type k for the i-th parcel; M is the size of the neighborhood window used for calculating land use density; and $\sum_{M\times M} con(c_i = k)$ represents the area of parcels with land use type k within an $M \times M$ neighborhood window.

To construct the objective function, this study employs RFR to fit the functions f_H and f_{LST} in equation (6). RFR is a supervised ensemble method based on decision trees, which has been applied in various studies (Yao et al., 2017). RFR randomly selects samples and features from the training dataset, handles high-dimensional feature data, and addresses multicollinearity issues among features. The RFR outputs a given parcel's average building height within neighborhood and LST. We constructed a separate RFR model for each type of land use. When fitting f_H, the *SV* and the *LUD* are used as features; when fitting f_{LST}, the *SV*, *LUD*, and the average building height within the neighborhood are used as features. We applied coefficient of determination (R^2), and root mean squared error (RMSE) as the predictive accuracy. The accuracy of RFR is shown in Table A3.

(2) Maximizing suitability

In this study, the suitability of a parcel is quantified based on the land use development potential output by the PLUS model in equation (8).

$$Max \sum_{k=1}^{K} \sum_{i=1}^{N} I(x_i = k) suit_i^k \tag{8}$$

where i represents the i-th land parcel; k represents the k-th type of land use; N is the number of land parcels in the PDA; K is the number of parcel types; $I(\bullet)$ is an indicator function; x_i denotes the land use type of the i-th parcel; $suit_i^k$ represents the suitability of the k-th type of land use for the i-th parcel.

3.3.2. Particle swarm representation

In the particle swarm optimization (PSO) algorithm, a particle represents a solution in the solution space. Each particle moves through the solution space at a certain velocity, which is updated based on the particle's personal best solution and the swarm's global best solution (Wang et al., 2018).

As shown in Fig. 6, since this study only optimizes the land parcels within the PDA, first use the mask of the non-PDA to extract the land use map in the non-PDA, then calculate the quantity of the land use types in the non-PDA, and subtract it from the land use demand in 2030 to obtain the quantity of the land use types in the PDA. A particle is represented as a land parcel sequence. Replicate the land parcel sequence N times to generate the particle swarm as an N × M matrix, where N is the swarm size, and M is the number of land parcels in the PDA. For each particle in the swarm, the order of land parcels within the swarm is randomly shuffled to serve as the initial particle swarm.

3.3.3. Particle swarm update

In the PSO, each particle's fitness is assessed using the objective function. The best solution found by each particle in its history is known as the personal best, P_{best}, and the best solution among all particles is known as the global best, G_{best}. Each particle is updated based on P_{best} and G_{best}, completing the optimization process iteratively.

This study aims to mitigate the UHI effect by reallocating the spatial positions of land parcels. In geographical space, the positions of land parcels are discrete. However, the original PSO was initially designed for optimizing continuous functions, making it not directly applicable to this study. (Kang-Ping et al., 2003) introduced the concepts of Swap Operator (SO) and Swap Sequence (SS) and redefined some operators to make PSO compatible with discrete combinatorial optimization problems. The update formulas for a single particle are provided in equations (9) and (10):

$$V_{t+1} = V_t \oplus \alpha(P_{best} - X_t) \oplus \beta(G_{best} - X_t) \tag{9}$$

$$X_{t+1} = X_t + V_{t+1} \tag{10}$$

where the operator $\oplus$ is defined as the combination of two swap sequences into a new swap sequence; t represents the iteration count; V_t represents the swap sequence at iteration t; $(P_{best} - X_t)$ is defined as the swap sequence of the particle at iteration t relative to its personal best solution; $(G_{best} - X_t)$ is defined as the swap sequence of the particle at iteration t relative to the global best solution; acceleration constant α and β are random numbers between 0 and 1, representing the probability of applying the swap sequences, where larger α indicates a greater influence of the particle's personal best on the particle, and larger β indicates a greater influence of the global best on the particle; equation (10) defines the application of the swap sequence V_{t+1} to particle X_t to obtain the new particle X_{t+1}.

This study employs a non-dominated sorting algorithm (Deb et al., 2000) to select P_{best} and G_{best}. Specifically, for P_{best}, if the particle at iteration t performs better on both objective functions than the particle at iteration $t-1$, then this particle is used to update P_{best}. Otherwise, one is randomly selected between the two as P_{best}. As for G_{best}, the first step is to identify the non-dominated set of solutions among the particles in the swarm and then select the particle with the highest crowding distance from this non-dominated set as G_{best}. The formula for crowding distance is given in equation (11):

$$CD_i = \frac{|f_1(x_{i+1}) - f_1(x_{i-1})|}{f_1(x_{max}) - f_1(x_{min})} + \frac{|f_2(x_{i+1}) - f_2(x_{i-1})|}{f_2(x_{max}) - f_2(x_{min})} \tag{11}$$

where CD_i is the crowding distance of the i-th particle; $f_1(\cdot)$ and $f_2(\cdot)$ are the two objective functions; x_i represents the i-th particle; x_{max} represents the particle that achieves the maximum value on the objective function; and x_{min} represents the particle that achieves the minimum value on the objective function.

Fig. 7 illustrates the update method for a particle in the particle swarm. The swap sequence is obtained based on G_{best} and P_{best}, which contains swap operators. A swap operator is a pair of numbers that indicate the indices in the parcel sequence to be swapped. After executing the swap operations sequentially according to the swap operators, the land parcel sequence within the particle should exactly match the best solution. The swap sequence SS_P is extracted from the current particle and its personal best solution P_{best}, and the swap sequence SS_G is extracted from the current particle and the global best solution G_{best}.

The swap sequences SS_P and SS_G are combined to obtain V_{t+1}. Then, execute the swap sequence V_{t+1} sequentially on the particle X_t. Execute the swap operator in the swap sequence with probability, and the probability is calculated by equation (12):

$$swapprobability = \max(P_1, P_2) \times accelerationconstant \tag{12}$$

where P_1 and P_2 are the likelihood values of the two land parcels in the PDA; if the swap operator is from the SS_P, the *accelerationconstant* is α; if

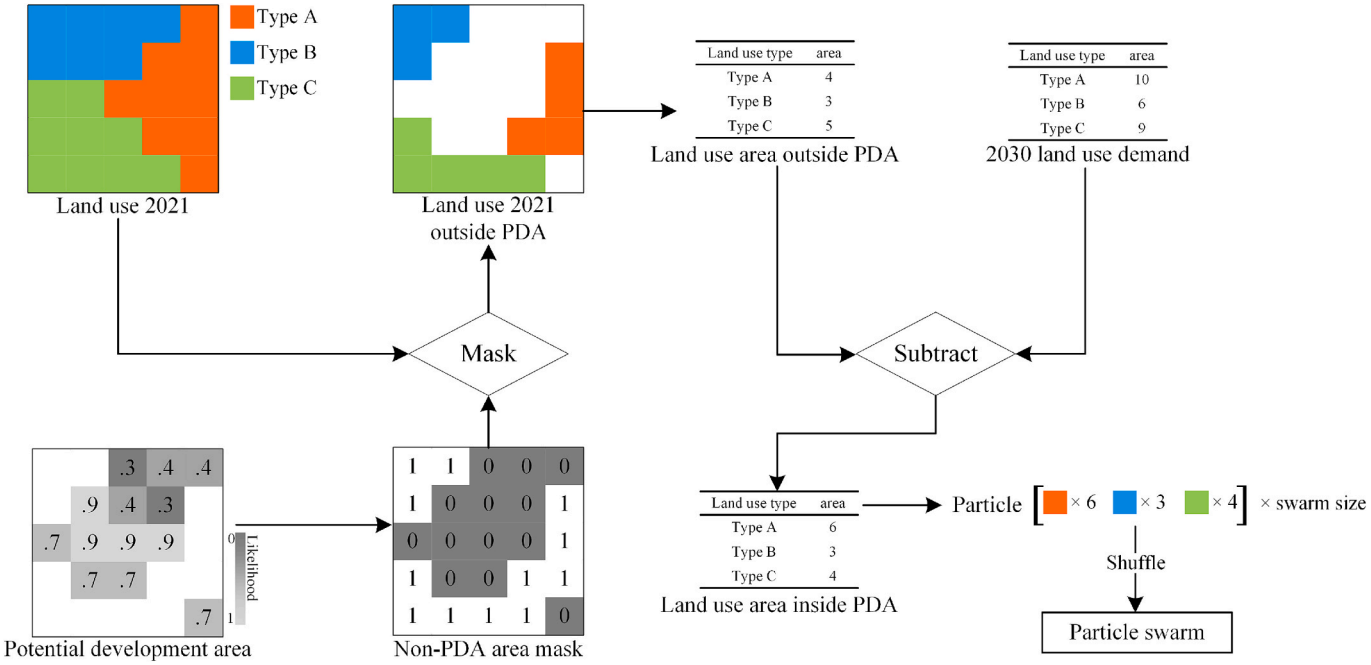

Fig. 6. Particle representation and particle swarm generation.

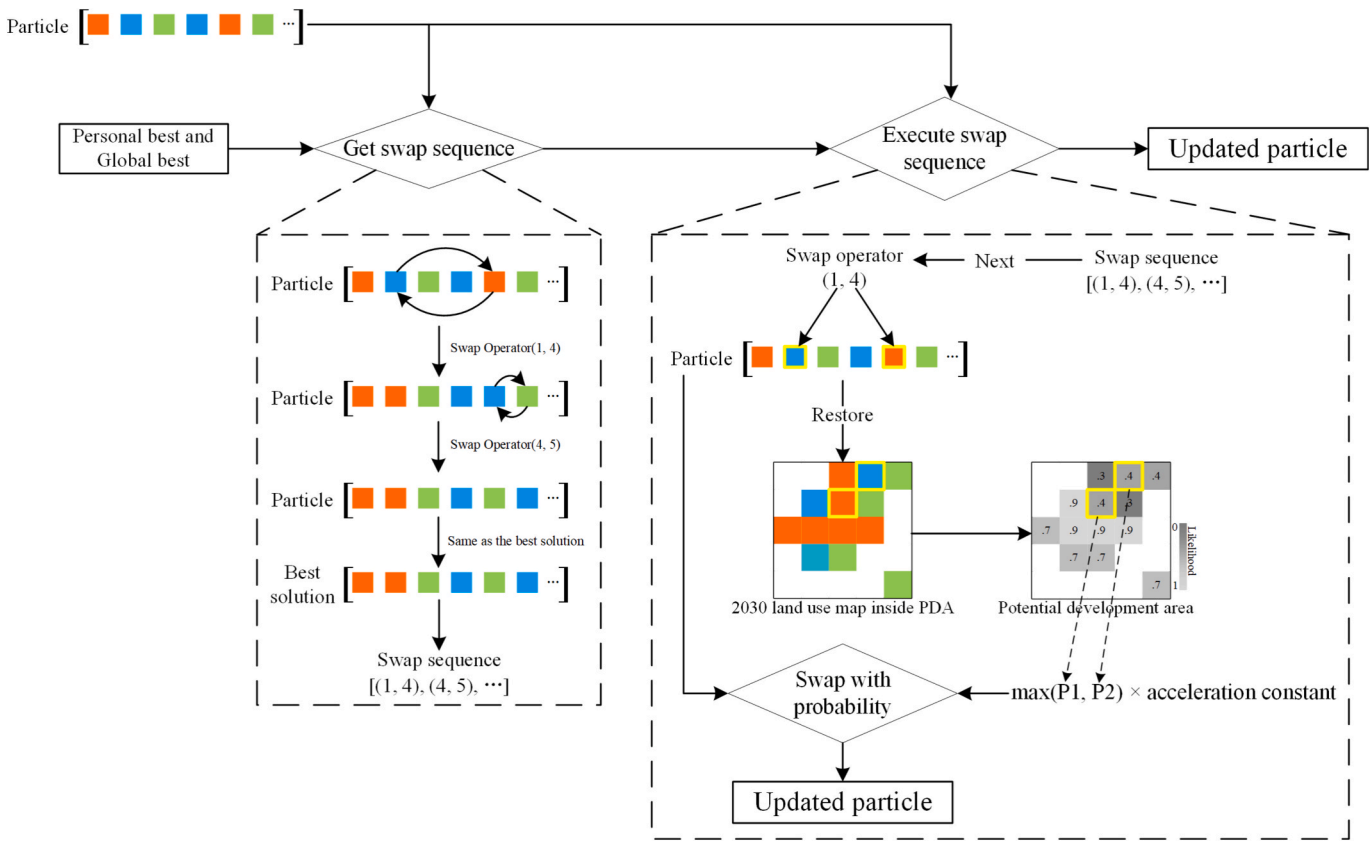

Fig. 7. Flowchart for extracting swap sequence.

it is from SS_G, the *accelerationconstant* is β. Once all swap operators have been executed, a new solution sequence X_{t+1} is obtained. The land parcel sequence in X_{t+1} is then restored to the land use map in spatial order from left to bottom and top to bottom, resulting in the optimized spatial structure of land use.

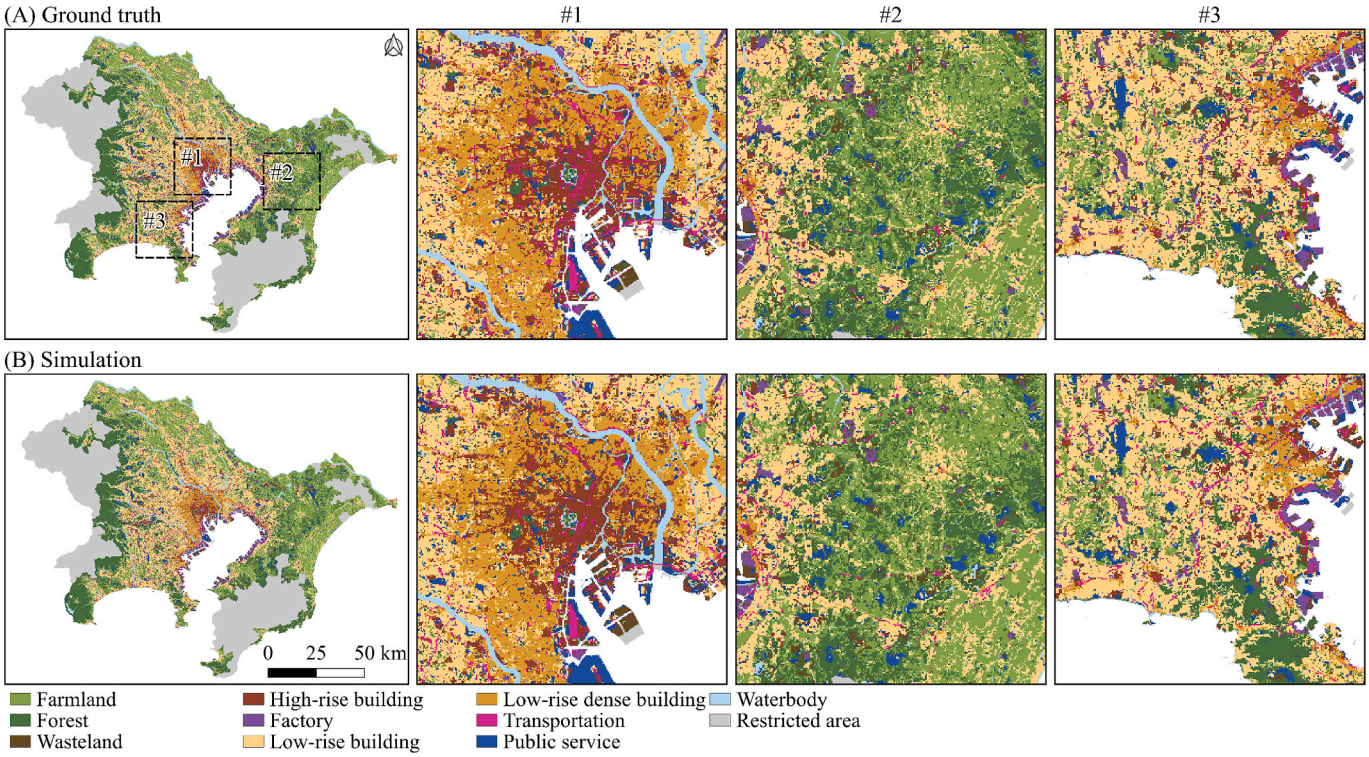

Fig. 8. Land use map (a) and land use simulation map (b) in the TMA.

4. Result

The proposed 3DLS-PO model is used to allocate spatial structure of land use to mitigate the UHI effect. We conducted experiments in the TMA under SSP scenarios and compared the changes in LST, average building height, and spatial structure of land use between initial and optimized state. Finally, we examined the changes in heatstroke incidents in Tokyo based on the optimization results to highlight the application of the 3DLS-PO model.

4.1. Simulating 2021 land use using PLUS in the TMA

This study uses the PLUS model to simulate the spatial structure of land use of the TMA in 2030. Before making predictions, we need to calibrate the PLUS model. The land use data from 2009 for the TMA was used as the initial layer to simulate the spatial structure of land use in 2021. Fig. 8 shows the simulation results and details of area #1, #2, and #3. We evaluated the model using the Kappa coefficient, FoM, and overall accuracy. The final Kappa coefficient was 0.88, the FoM metric was 0.20, and the overall accuracy was 0.91, indicating high precision. Moreover, we compared 15 landscape metrics (Liang et al., 2021) between the ground truth and simulation results (Table A3). While most landscape metrics showed small differences, the number of patches exhibited a substantial disparity. This disparity is primarily due to the land use simulation incorporating neighborhood influence, a factor that reduces land fragmentation.

4.2. Predicting 2030 potential development area under SSP scenarios

This study selects three scenarios to predict PDA for 2030: SSP1, SSP2, and SSP5. SSP1 is the Sustainable Development scenario that ensures urban development within a healthy ecological environment. SSP2 is the Middle of the Road scenario, where urban development does not significantly deviate from historical patterns. The difference between the SSP1 and SSP2 scenarios is that the SSP1 scenario maintains economic growth while controlling population growth and increasing technological investment. SSP5 is the Fossil-Fueled Development scenario, where the economy and technology in the region develop rapidly.

To forecast the 2030 land use demand under SSP scenarios, this study uses the demographic yearbook and 2021 land use data to calculate the per capita land area. Based on the per capita area and the forecasted 2030 population, the land use demand for all types is calculated. Table 4 presents the land use demand for the TMA in 2030 under the SSP1, SSP2, and SSP5 scenarios. Compared with 2021, the area of urban land use in each scenario is projected to increase, while the area of non-urban land use (FL, For and WL) is projected to decrease. The largest urban growth area is projected under the SSP5 scenario, followed by SSP1 and SSP2.

Table 4
Per capita area of various land use types and the increase in area under SSPs in 2030 compared to 2021.

Type	Area per capita (10^{-4} km^2/ people)	2021 area (km^2)	Increased area by 2030 compared to 2021 (km^2)		
			SSP1	SSP2	SSP5
FL	/	2325.53	−104.29	−24.35	−154.99
For	/	1960.83	−19.77	−4.62	−29.38
WL	/	293.25	−16.87	−3.94	−25.07
HRB	8.82	324.09	9.64	2.25	14.33
Fac	5.08	186.86	5.56	1.30	8.26
LRB	85.67	3148.34	93.69	21.88	139.24
LRDB	8.94	328.70	9.78	2.28	14.54
Trans	6.65	244.54	7.28	1.70	10.81
PS	13.69	503.36	14.98	3.50	22.26

Note: FL (farmland); For (forest); WL (wasteland); HRB (high-rise building); Fac (factory); LRB (low-rise building); LRDB (low-rise dense building); Trans (transportation); PS (public service).

Although SSP2 represents the Middle of the Road scenario, its lowest population growth before 2030 results in the smallest urban growth area among these scenarios, as confirmed by Chen et al. (2020).

Based on the 2030 land use demand, the calibrated PLUS model was used to simulate the spatial structures of land use for 2030 10 times. We extracted the areas that changed compared to 2021. Fig. 9 shows the land parcels that will change in 2030, with a higher likelihood value indicating that the parcel is more likely to change in 2030. The most significant changes occur under the SSP5 scenario, followed by SSP1 and then SSP2. Area #1 represents the core area of TMA, with changes primarily occurring in the surrounding areas. Area #2 is a suburb far from the core. As illustrated in Fig. 9, the PDA exhibits a patchy distribution across the study area, characterized by high likelihood values in the center of the patches and lower values at the edges. Moreover, the locations and shapes of the PDA patches are similar across different SSP scenarios. However, under scenarios with more pronounced changes, the patches display higher likelihood values. For example, as shown in the areas within the black dotted circles, the PDA patches under the SSP5 scenario appear redder than those under the SSP1 and SSP2 scenarios. The area for each land use type within the PDA is calculated by subtracting the area outside the PDA from the SSP scenario area in Table 4. The results are shown in Table 5. Under the SSP2 scenario, the area of each land use type is smallest, followed by SSP1 and SSP5.

4.3. Optimizing urban land use to mitigate UHI effect under SSP scenarios

In this study, under the SSP5 scenario, we obtained the result of optimized state at different window sizes (5 × 5, 7 × 7, 9 × 9, and 11 × 11) (Table A3). The results show that land use density integrated within a 9 × 9 window size achieves maximum optimization effects. Then, we also obtained the result of optimized state at different land use resolutions (100 m, 200 m, and 300 m) under the optimal window size (Table A4). The results indicated that finer resolution enhances the optimization effect for LST but decreases it for land suitability. However, coarser resolution leads to more mixed pixels, which affects the reliability of the optimization results and hinders urban planning decisions. Finally, the optimal parameter combination was determined to be a 9 × 9 window size and a 100 m land use resolution.

Land parcels that changed between 2021 and 2030 were selected for optimization. The goal of the optimization was to maximize the negative sum of LST for all targeted parcels while considering their suitability. After the optimization process, the optimal solution was compared with the initial state of land use (as shown in Table 6), demonstrating significant improvements in both optimization objectives. Under the SSP5 scenario, LST saw the largest decrease at 5.18 %, followed by SSP1 at 4.60 %, with SSP2 experiencing the smallest decrease at 2.34 %. Fig. 10 illustrates the changes in LST within the PDA after optimization. We used the Zonal statistics tool in QGIS 3.34 to highlight the changed areas.

Spatially, we compared the kernel density of land use pixels within the PDA between the initial state (where land use pixels were randomly distributed within the PDA) and the optimized state to highlight the areas that were optimized, as shown in Fig. 11. Based on the optimized spatial locations of different land use types under each SSP scenario, we can identify the urban spatial form with the optimal UHI effect to assist urban planning. Since the PDA area under the SSP5 scenario is the largest (Table 5), it exhibits the greatest change in kernel density, followed by SSP1 and SSP2. The land use type with the most significant change in kernel density is LRB, as it is the primary land use type within the PDA. HRB was primarily allocated to the periphery of the core area of the TMA and northern Chiba, balancing the two optimization objectives of this study—maximizing suitability and minimizing LST. Fac was allocated to suburban areas far from the urban core and near water bodies, as both locations are typically associated with lower LST. LRB and LRDB, as the primary residential land use types, were allocated throughout the study area. Finally, green spaces were scattered across

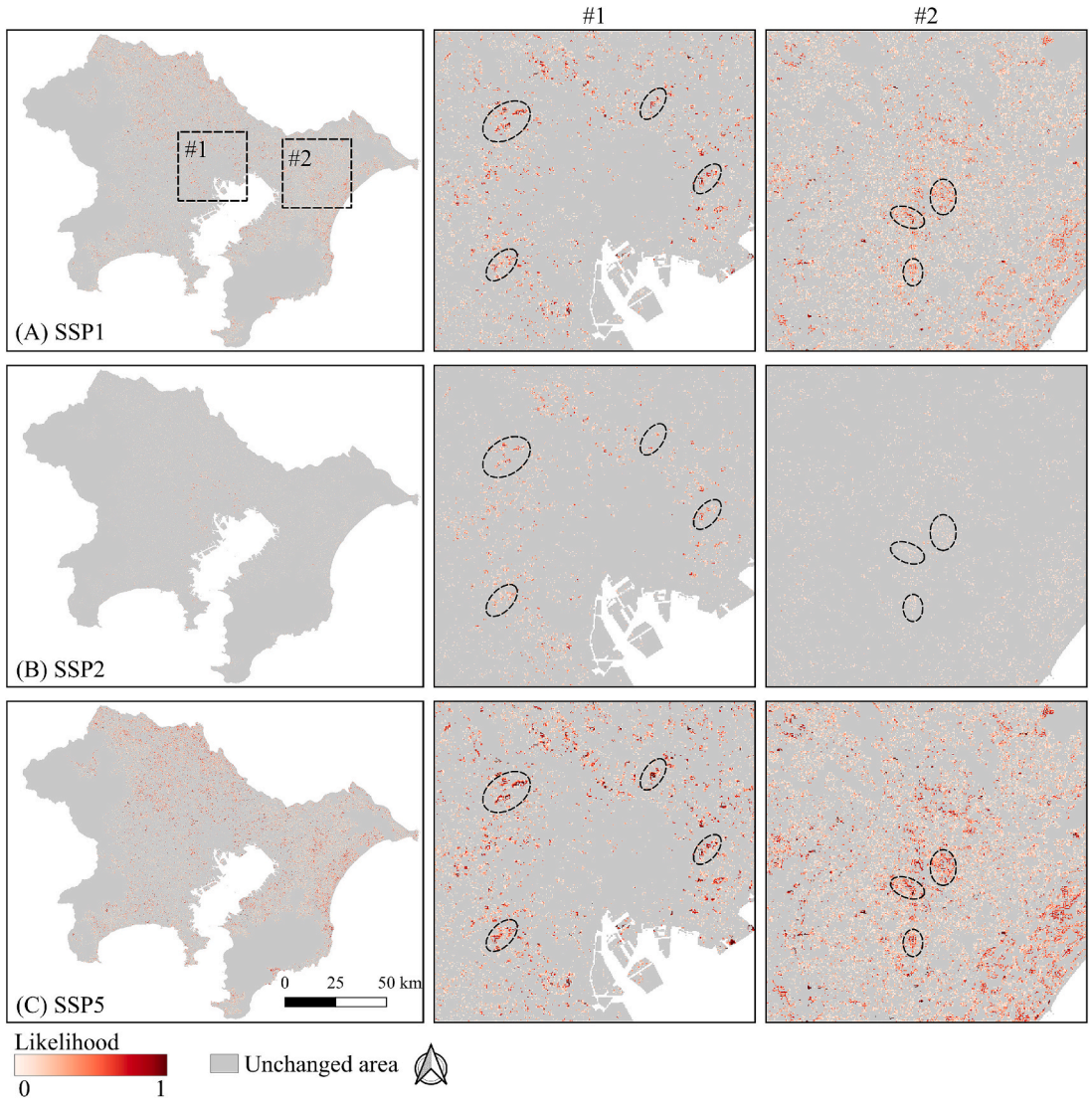

Fig. 9. Changes in land parcels for 10 simulations under SSPs.

Table 5
Area of each land use within the 2030 PDA (Km^2).

Scenario	FL	For	WL	HRB	Fac	LRB	LRDB	Trans	PS
SSP1	652.13	263.01	89.02	9.64	5.56	613.35	48.60	7.28	14.98
SSP2	183.25	36.94	25.17	2.25	1.30	104.25	46.84	1.70	3.50
SSP5	731.01	338.93	101.40	14.33	10.22	813.93	64.34	10.81	22.26

Note: FL (farmland); For (forest); WL (wasteland); HRB (high-rise building); Fac (factory); LRB (low-rise building); LRDB (low-rise dense building); Trans (transportation); PS (public service).

Table 6
Comparison of objective functions between initial and optimized state in each scenario.

Scenario	LST (℃)		Suitability	
	Initial	Optimized	Initial	Optimized
SSP1	47.22	45.05	59.24	60.84
SSP2	48.82	47.68	45.78	47.73
SSP5	45.72	43.35	58.62	60.03

the study area to exert their cooling effect.

4.4. Preventing heatstroke incidents in Tokyo

To demonstrate the practical implication of the optimized result, this section calculated the change rate of heatstroke incidents. O'Malley & Kikumoto (2021) examined the quantitative relationship between LST and heatstroke incident rates in Tokyo at the ward level. Hence, we selected Tokyo as a case study area to calculate the average LST change rates of wards and estimate the variations in heatstroke incident rates between initial and optimized state, as shown in Fig. 12. By incorporating the ward-level population data, we estimated the change rate of heatstroke incidents after optimizing the spatial structure of urban land

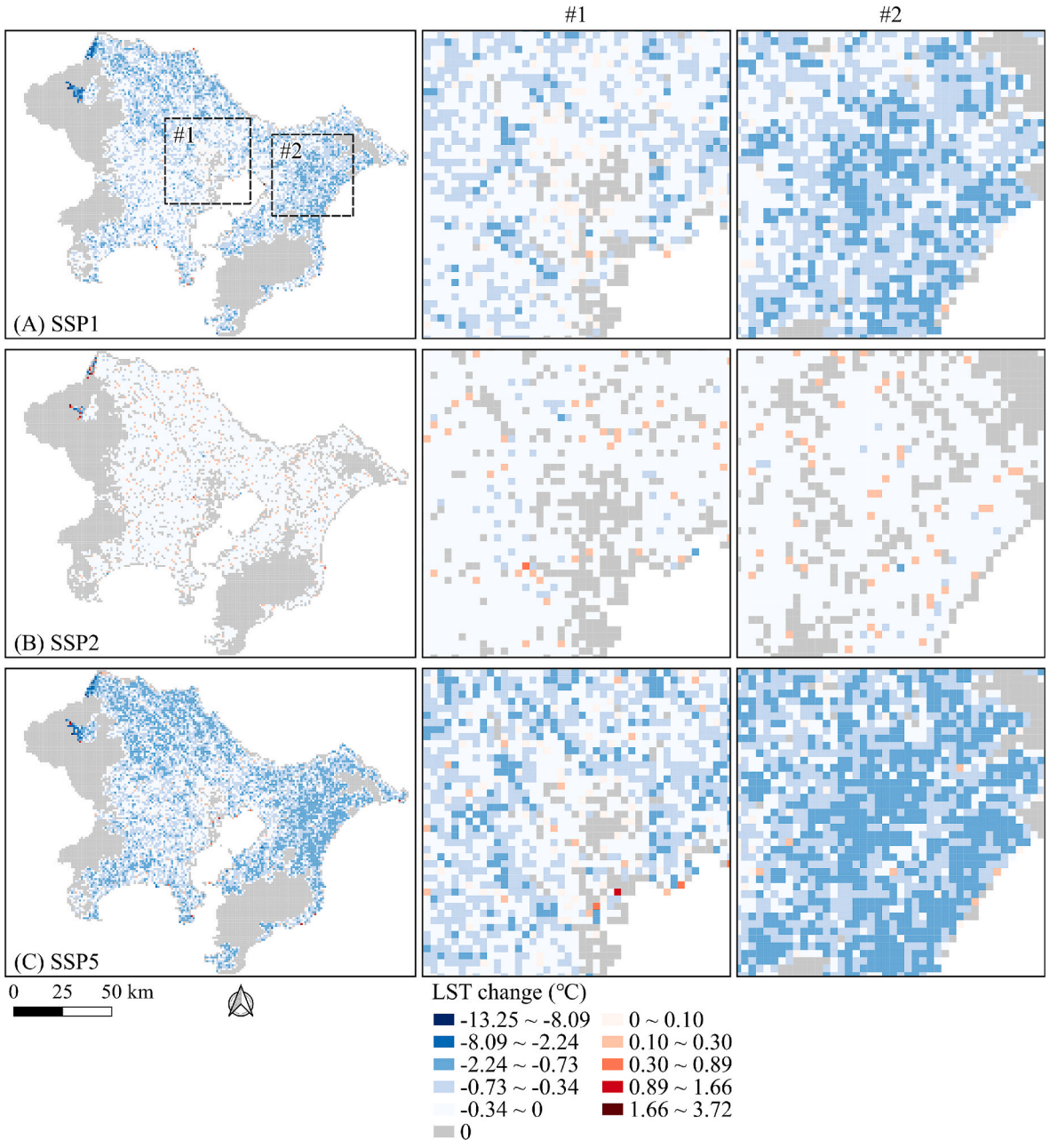

Fig. 10. LST change between initial and optimized state within PDA.

use under SSPs. As shown in Fig. 12, the areas with a significant decline in heatstroke incidents are mainly concentrated in the middle of Tokyo, especially Kokubunji and Musashino wards, followed by Kiyose, Suginami, and Setagaya wards; the heatstroke incidents also decreased significantly under SSP1 and SSP5 scenarios. These wards are mainly distributed with low-rise buildings and low-rise dense buildings (Fig. 1), where large population concentration exacerbates heat vulnerability. In contrast, the minimal change rate of heatstroke incidents is estimated in the east of Tokyo, such as Chiyoda, Minato, and Chuo wards. The land parcels of these wards have rarely changed as they are Tokyo's political, economic, and cultural center (Fig. 9).

We also applied a geographical detector to investigate further the contribution of each land use type to the change rate of heatstroke incidents (Song et al., 2020). In this geographical detector, we used land use kernel density change as the independent variable and the change rate of heatstroke incidents as the dependent variable. As shown in Table 7, the results reveal differences across the SSP scenarios. Under the SSP1 scenario, the top three contributors to the change rate of heatstroke incidents are HRB, LRDB, and Trans, which are closely associated with urban environments. In contrast, under the SSP2 scenario, the highest contributions come from FL, WL, and For, indicating that in a more moderate development scenario, the thermal impact of rural land transformations plays a more critical role. Under the SSP5 scenario, the top 3 contributors are PS, WL, and Trans. This result may reflect the more intensive urban expansion and infrastructure development associated with high-emission, where heat exposure in public service and transportation-related areas becomes more critical.

5. Discussion

5.1. Policy implications

As the UHI effect threatens human health, mitigating the UHI effects under various scenarios is of significant practical importance for future

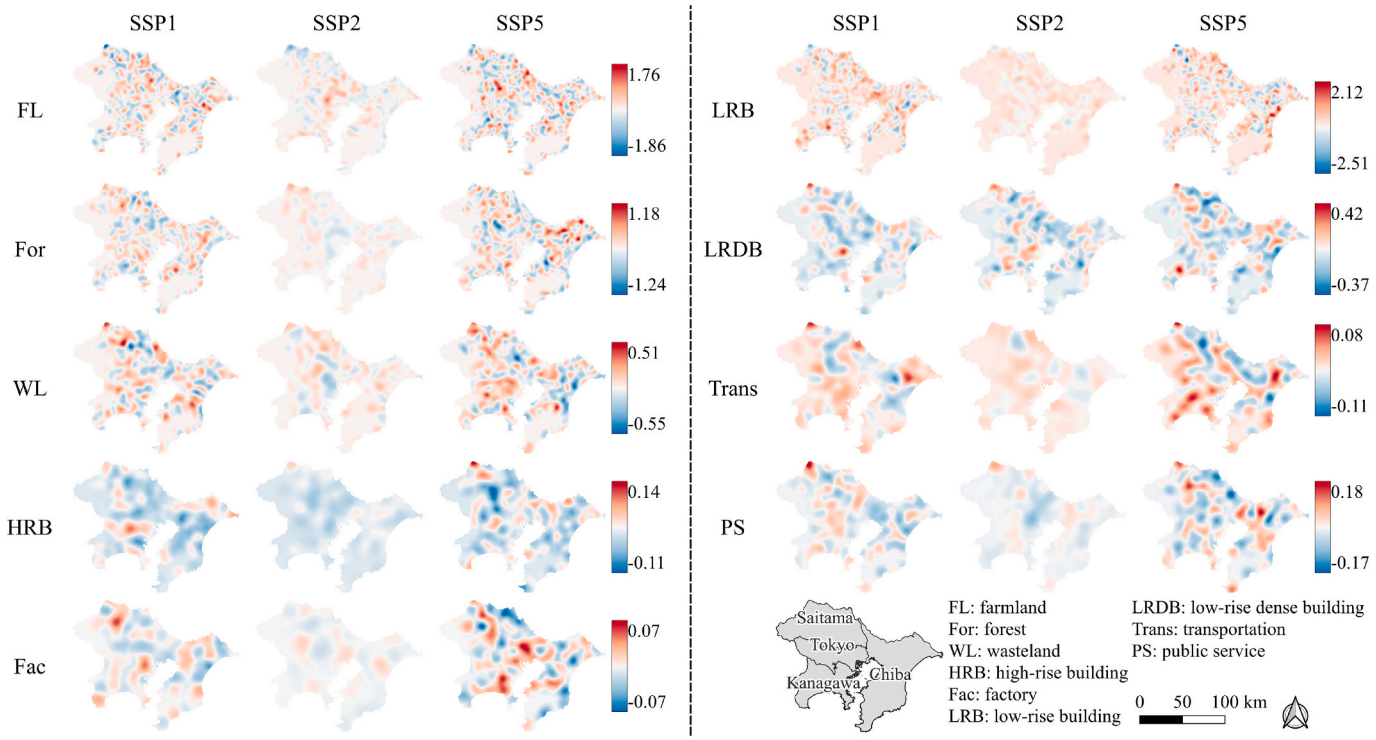

Fig. 11. Change in kernel density of land parcels by comparing the kernel density of land parcels in the initial state and the optimized state.

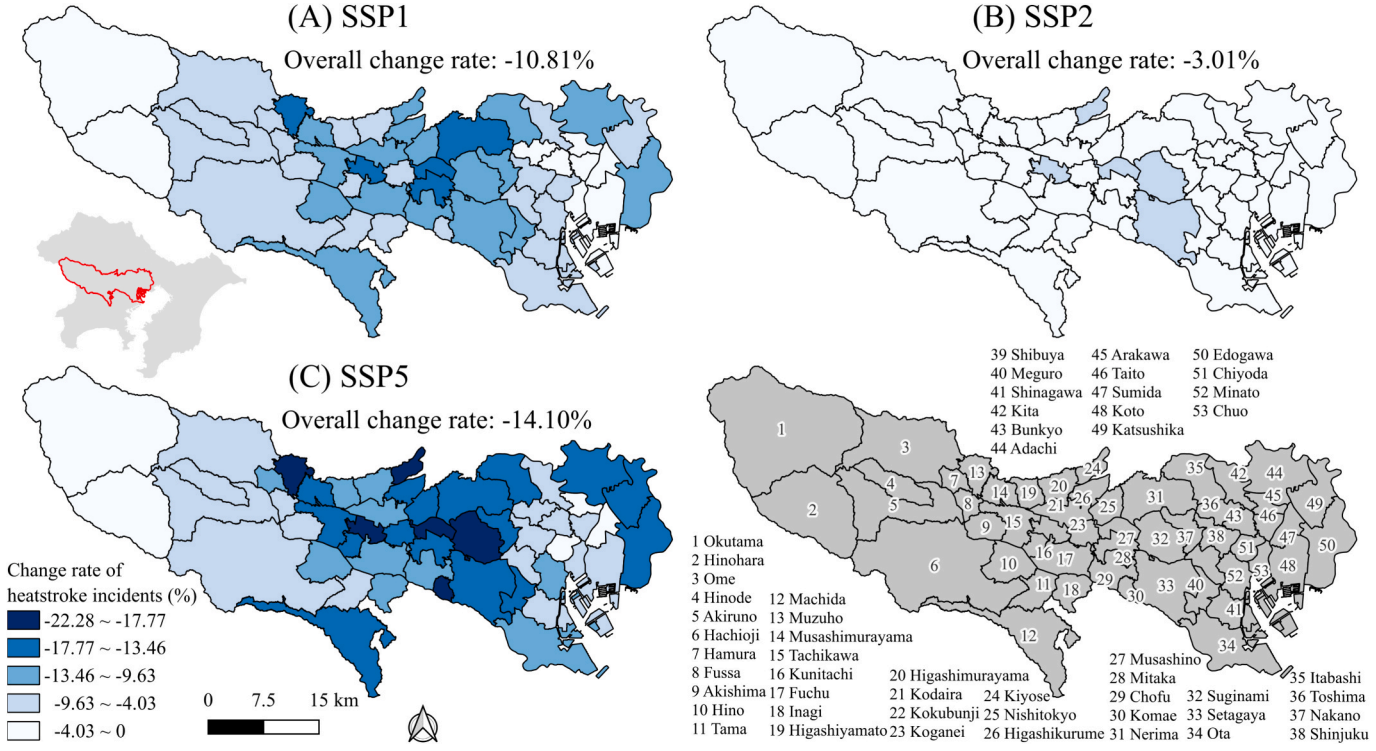

Fig. 12. Change rate of heatstroke incidents in Tokyo between initial and optimized state.

urban planning and climate adaptation planning (Parsaee et al., 2019). With rapid urbanization, the expansion of mega-cities has gradually slowed down, particularly in the city centers where available land resources are extremely limited. It is increasingly challenging to reduce LST in the city centers by constructing new urban land parcels with a cooling effect (Masoudi et al., 2021). As urban renewal has become a major development strategy for mega-cities (He, Zhang, et al., 2023), optimizing the spatial structure of land use has emerged as a practical approach to mitigate the UHI effects. Incorporating the urban three-dimensional landscapes into the optimization model is necessary as they strongly relate to the UHI effect (S. Cao et al., 2022; Wu et al., 2022; Zhu et al., 2023). Therefore, the 3DLS-PO model can be used as an

Table 7
Contributions of land use kernel density change to change rate of heatstroke incidents.

Land use	SSP1	SSP2	SSP5
FL	0.17	0.59	0.26
For	0.34	0.42	0.19
WL	0.35	0.43	0.35
HRB	0.44	0.18	0.16
Fac	0.18	0.30	0.22
LRB	0.37	0.20	0.23
LRDB	0.44	0.33	0.25
Trans	0.39	0.29	0.28
PS	0.22	0.33	0.39

Note: FL (farmland); For (forest); WL (wasteland); HRB (high-rise building); Fac (factory); LRB (low-rise building); LRDB (low-rise dense building); Trans (transportation); PS (public service).

efficient supporting tool for policymaking, as it can simulate UHI-related indicators to mitigate UHI. We can estimate the number of reduced heatstroke incidents with the optimization results to provide evidence-based indicators for allocating public health resources. Besides, urban planners and policymakers can formulate and implement more comprehensive strategies to enhance the urban microclimate and strengthen urban resilience to climate change based on the optimization results, including constructing green buildings (He, 2019), allocating mixed-functional areas (Liang et al., 2024), and planning transportation infrastructure (A. Wang et al., 2024).

To effectively mitigate the UHI effect, it is crucial to propose region-specific policies tailored to the study area (Ferrario et al., 2024). This study mapped the changes in the kernel density of land use within the PDA between initial and optimized state (Fig. 11). First, HRB is currently mainly concentrated in the core area of the TMA (Fig. 1). Under the SSP1, SSP2, and SSP5 scenarios, the land use area of HRB is projected to increase by 9.64, 2.25, and 14.33 km^2 by 2030, respectively. These new HRBs are primarily allocated to the areas surrounding the TMA core area and northern Chiba. To further enhance its cooling effect and urban functionality, HRB should be integrated with LRB and LRDB in a mixed development pattern. Second, the Factory should be located near waterbodies and away from the city center, such as in northwestern Saitama, central and northern Chiba, and coastal areas of Kanagawa. Third, LRB, as the primary type of residential land, should be expanded toward suburban areas to avoid forming densely concentrated residential areas that are prone to high-LST (Y. Li et al., 2020), and medium-rise buildings with a higher floor area ratio (FAR) should be developed nearby. Finally, pocket parks and green spaces should be developed throughout the TMA to utilize their cooling effect fully.

5.2. Model contribution

Compared to traditional land use optimization models, the main contribution of the 3DLS-PO model can be concluded in three aspects: integration of three-dimensional spatial patterns, focused optimization of potential development areas (PDA), and broad applicability.

First, due to the lack of three-dimensional information on the land parcels, traditional land use optimization models were applied at the two-dimensional level (Ahmed et al., 2024; Qiu et al., 2023; Wardeh et al., 2022). This study innovatively incorporates building heights as crucial three-dimensional information into land use optimization. Given that the urban three-dimensional structure is closely related to the urban environment (Wang et al., 2021; Xu et al., 2021). The three-dimensional land use optimization results can better assist urban planners to comprehensively evaluate the impact of the optimized land use spatial structure on the UHI effect.

Second, traditional land use spatial optimization models usually randomly distribute all land parcels in the study area before optimization (Tong, Yang, et al., 2024). The 3DLS-PO model only optimizes the land use pixels in PDA, which brings two advantages: 1) Since the simulation of PDA is based on historical land use changes, the optimization results of 3DLS-PO, coupled with the historical laws of land use changes, will be more reasonable compared with the optimization results of traditional models. 2) The 3DLS-PO model has higher execution efficiency than the traditional model. We compared the execution efficiency in different optimization regions. The experimental results show that it takes 43 s to update the particle once if all the land parcels in the study area are optimized, but only 3 s (a 14-fold increase in efficiency) if only the land parcels in the PDA are optimized. The high efficiency could support land use spatial optimization in a larger spatial scale.

Third, although the 3DLS-PO model prioritizes reducing LST as the optimization objective, the framework of "identify PDA first, then optimize the spatial structure of land use within the PDA" can be transferred to other tasks such as controlling carbon emission or energy consumption.

5.3. Model assumptions and potential limitations

To complete three-dimensional land use optimization in TMA, the 3DLS-PO model has two assumptions due to the limitations of data acquisition and technology: 1) The 3DLS-PO model is a pixel-based model, assuming urban land use change occurs at the pixel level. Since the official land use data is pixel-based, each 100 × 100 m pixel represents a single land use type. However, in large metropolitan areas like the TMA, land use pattern is typically complex, characterized by irregularly shaped land parcels and often featuring mixed-use functions. As a result, the pixel-based optimization results obtained by the 3DLS-PO model may result in a fragmented land use pattern. 2) The 3DLS-PO model utilizes static spatial variables to fit LST, assuming they remain constant during the optimization process. However, fine-scale spatial variables related to human activities also significantly influence the UHI effect, such as energy consumption and traffic flow. Due to a lack of accessible open data sources, these dynamic spatial variables were not considered in the 3DLS-PO model. Ignoring the anthropogenic heat generated by human activities may lead to an underestimation of the UHI effect in certain regions.

Given that the 3DLS-PO model is constructed based on the aforementioned assumptions, we identify two potential limitations: 1) While the optimization results of the 3DLS-PO model are applicable for macro-level urban planning regulation, they may not adequately support fine-scale, functionally diverse policy interventions. The lack of parcel-level land use data and parcel-level optimization model restricts the 3DLS-PO model's ability to simulate the optimization process of irregular shaped land parcels. 2) The nonlinear relationship used to predict LST cannot fully capture the impact of human activities due to a lack of supporting data. This limitation could lead to an underestimation of the UHI effect in certain regions, thereby affecting the validity of the optimization results. The 3DLS-PO model results could not support formulating UHI mitigation strategies that require human-activity-based interventions.

5.4. Future works

Future improvements to the 3DLS-PO model should focus on two aspects, addressing its potential limitations: 1) The framework of the 3DLS-PO model can be extended to optimize parcel-level mixed urban land use structure. To better represent complex land use pattern, the model could transfer from a pixel-level to a parcel-level approach for simulating PDA. Developing an effective approach to optimizing irregular shaped land parcels is a technical challenge that needs to be addressed in the future. 2) Fine-scale human activity data can be integrated into the 3DLS-PO model. Since human activities significantly influence both land use change and the UHI effect, incorporating fine-scale data such as building-level electricity usage, GPS trajectories, and mobile phone signaling could enhance the simulation accuracy of the model for PDA and improve its interpretability for human activities.

This enhanced capability would support formulating more reasonable strategies to mitigate the UHI effect.

6. Conclusion

This study proposed a land use spatial optimization model, 3DLS-PO, by integrating the PLUS model and PSO algorithm to mitigate the UHI effect. The 3DLS-PO model focuses on optimizing only those land parcels expected to change and considers the urban three-dimensional landscapes during the optimization process. Based on the optimization results of future scenarios, decision-makers or urban planners can predict and evaluate the possible consequences of different urban planning policies before making decisions.

To validate the effectiveness of the 3DLS-PO model, we conducted experiments in the TMA under different SSPs. The PLUS model demonstrated satisfactory accuracy (Kappa = 0.88, FoM = 0.20) in proving the reliability of conversion rules. The optimization results indicate that under the SSP5 scenario, the optimized LST achieves the largest decrease of 5.18 % (45.72℃ to 43.35℃), followed by SSP1 and SSP2 with decreases of 4.60 % (47.22℃ to 45.05℃) and 2.34 % (48.82℃ to 47.68℃), respectively. In Tokyo, the number of heatstroke incidents decreased by 10.81 %, 3.01 %, and 14.10 % under SSP1, SSP2, and SSP5 scenarios, respectively. The spatial comparison of land use allocation reveals several strategies to mitigate UHI effects: decentralizing high-rise buildings to the TMA periphery, expanding low-rise housing into suburban areas, locating factories near waterbodies and away from the city center, and distributing green spaces evenly to enhance cooling effects. The proposed 3DLS-PO framework offers a methodological foundation for sustainable urban planning and provides novel insights for mitigating UHI effect through three-dimension land use spatial structure optimization.

CRediT authorship contribution statement

Shiyu Xiao: Writing – original draft, Visualization, Validation, Methodology, Investigation, Formal analysis, Data curation. **Jialyu He:** Writing – original draft, Visualization, Validation, Methodology, Investigation, Formal analysis, Data curation. **Yao Yao:** Visualization, Validation, Resources, Investigation, Formal analysis, Data curation. **Xun Liang:** Validation, Resources, Methodology, Formal analysis. **Xia Li:** Writing – review & editing, Supervision, Project administration, Funding acquisition, Conceptualization.

Acknowledgments

This study was supported by the Key National Natural Science Foundation of China (Grant No. 42130107 and 42471491) and the Open Project of Hunan Geospatial Information Engineering and Technology Research Center (Grant No. HNGIET2025004).

Appendix A. Supplementary material

Supplementary data to this article can be found online at https://doi.org/10.1016/j.landurbplan.2025.105490.

Data availability

I have shared the link to my data at the manuscript.

References

Ahmed, N. M., Altamura, P., Giampaoletti, M., Hemeida, F. A., & Mohamed, A. F. A. (2024). Optimizing human thermal comfort and mitigating the urban heat island effect on public open spaces in Rome, Italy through sustainable design strategies. *Scientific Reports, 14*(1), 19931. https://doi.org/10.1038/s41598-024-65794-8

Akkose, G., Meral Akgul, C., & Dino, I. G. (2021). Educational building retrofit under climate change and urban heat island effect. *Journal of Building Engineering, 40*, Article 102294. https://doi.org/10.1016/j.jobe.2021.102294

Cao, M., Chang, L., Ma, S., Zhao, Z., Wu, K., Hu, X.,…Chen, M. (2022). Multi-Scenario Simulation of Land Use for Sustainable Development Goals. *IEEE Journal of Selected Topics in Applied Earth Observations and Remote Sensing, 15*, 2119-2127. doi:10.1109/JSTARS.2022.3152904.

Cao, S., Weng, Q., & Lu, L. (2022). Distinctive roles of two- and three-dimensional urban structures in surface urban heat islands over the conterminous United States. *Urban Climate, 44*, Article 101230. https://doi.org/10.1016/j.uclim.2022.101230

Che, Y., Li, X., Liu, X., Wang, Y., Liao, W., Zheng, X.,…Dai, Y. (2024). 3D-GloBFP: the first global three-dimensional building footprint dataset. *Earth Syst. Sci. Data*, *16*(11), 5357-5374. doi:10.5194/essd-16-5357-2024.

Chen, G., Li, X., Liu, X., Chen, Y., Liang, X., Leng, J.,…Huang, K. (2020). Global projections of future urban land expansion under shared socioeconomic pathways. *Nature Communications*, *11*(1), 537. doi:10.1038/s41467-020-14386-x.

Chen, Y., Li, X., Liu, X., & Ai, B. (2014). Modeling urban land-use dynamics in a fast developing city using the modified logistic cellular automaton with a patch-based simulation strategy. *International Journal of Geographical Information Science, 28*(2), 234–255. https://doi.org/10.1080/13658816.2013.831868

Chen, Y., Zhao, S., & Pei, L. (2024). Comparing the warming effects of different urban forms under projected climate change in China's Guangdong-Hong Kong-Macau Greater Bay Area. *Urban Climate, 53*, Article 101824. https://doi.org/10.1016/j.uclim.2024.101824

Coseo, P., & Larsen, L. (2014). How factors of land use/land cover, building configuration, and adjacent heat sources and sinks explain Urban Heat Islands in Chicago. *Landscape and Urban Planning, 125*, 117–129. https://doi.org/10.1016/j.landurbplan.2014.02.019

Deb, K., Agrawal, S., Pratap, A., & Meyarivan, T. (2000, 2000//). A Fast Elitist Non-dominated Sorting Genetic Algorithm for Multi-objective Optimization: NSGA-II. Parallel Problem Solving from Nature PPSN VI, Berlin, Heidelberg.

Du, G., Joo, S. K., Liang, Y., & Managi, S. (2018). A comparative approach to modelling multiple urban land use changes using tree-based methods and cellular automata: The case of Greater Tokyo Area. *International Journal of Geographical Information Science, 32*(4), 757–782. https://doi.org/10.1080/13658816.2017.1410550

Ferrario, F., Mourato, J. M., Rodrigues, M. S., & Dias, L. F. (2024). Evaluating Nature-based Solutions as urban resilience and climate adaptation tools: A meta-analysis of their benefits on heatwaves and floods. *Science of The Total Environment, 950*, Article 175179. https://doi.org/10.1016/j.scitotenv.2024.175179

Futcher, J., Mills, G., Emmanuel, R., & Korolija, I. (2017). Creating sustainable cities one building at a time: Towards an integrated urban design framework. *Cities, 66*, 63–71. https://doi.org/10.1016/j.cities.2017.03.009

Han, Y., & Jia, H. (2017). Simulating the spatial dynamics of urban growth with an integrated modeling approach: A case study of Foshan, China. *Ecological Modelling, 353*, 107–116. https://doi.org/10.1016/j.ecolmodel.2016.04.005

He, B.-J. (2019). Towards the next generation of green building for urban heat island mitigation: Zero UHI impact building. *Sustainable Cities and Society, 50*, Article 101647. https://doi.org/10.1016/j.scs.2019.101647

He, J., Liu, P., & Li, X. (2023). Modeling multi-type urban landscape dynamics along the horizontal and vertical dimensions. *Landscape and Urban Planning, 233*, Article 104683. https://doi.org/10.1016/j.landurbplan.2023.104683

He, J., Zhang, J., Yao, Y., & Li, X. (2023). Extracting human perceptions from street view images for better assessing urban renewal potential. *Cities, 134*, Article 104189. https://doi.org/10.1016/j.cities.2023.104189

Hu, C., Zhang, M., Huang, G., Li, Z., Sun, Y., & Zhao, J. (2024). Tracking the impact of the land cover change on the spatial-temporal distribution of the thermal comfort: Insights from the Qinhuai River Basin, China. *Sustainable Cities and Society, 116*, Article 105916. https://doi.org/10.1016/j.scs.2024.105916

Huang, X., & Wang, Y. (2019). Investigating the effects of 3D urban morphology on the surface urban heat island effect in urban functional zones by using high-resolution remote sensing data: A case study of Wuhan, Central China. *ISPRS Journal of Photogrammetry and Remote Sensing, 152*, 119–131. https://doi.org/10.1016/j.isprsjprs.2019.04.010

Kang-Ping, W., Lan, H., Chun-Guang, Z., & Wei, P. (2003, 5-5 Nov. 2003). Particle swarm optimization for traveling salesman problem. Proceedings of the 2003 International Conference on Machine Learning and Cybernetics (IEEE Cat. No.03EX693).

Kennedy, J., & Eberhart, R. (1995, 27 Nov.-1 Dec. 1995). Particle swarm optimization. Proceedings of ICNN'95 - International Conference on Neural Networks,.

Kikumoto, H., Ooka, R., & Arima, Y. (2016). A study of urban thermal environment in Tokyo in summer of the 2030s under influence of global warming. *Energy and Buildings, 114*, 54–61. https://doi.org/10.1016/j.enbuild.2015.07.033

Li, S., Wang, Z., Wu, X., Zeng, Z., Shen, P., & Lai, C. (2022). A novel spatial optimization approach for the cost-effectiveness improvement of LID practices based on SWMM-FTC. *Journal of Environmental Management, 307*, Article 114574. https://doi.org/10.1016/j.jenvman.2022.114574

Li, X., Peoples, J., Huang, Z., Zhao, Z., Qiu, J., & Ruan, X. (2020). Full daytime sub-ambient radiative cooling in commercial-like paints with high figure of merit. *Cell Reports Physical Science, 1*(10), Article 100221. https://doi.org/10.1016/j.xcrp.2020.100221

Li, X., & Zhou, W. (2019). Optimizing urban greenspace spatial pattern to mitigate urban heat island effects: Extending understanding from local to the city scale. *Urban Forestry & Urban Greening, 41*, 255–263. https://doi.org/10.1016/j.ufug.2019.04.008

Li, Y., Schubert, S., Kropp, J. P., & Rybski, D. (2020). On the influence of density and morphology on the Urban Heat Island intensity. *Nature Communications, 11*(1), 2647. https://doi.org/10.1038/s41467-020-16461-9

Liang, X., Guan, Q., Clarke, K. C., Liu, S., Wang, B., & Yao, Y. (2021). Understanding the drivers of sustainable land expansion using a patch-generating land use simulation (PLUS) model: A case study in Wuhan. *China. Computers, Environment and Urban Systems, 85*, Article 101569. https://doi.org/10.1016/j.compenvurbsys.2020.101569

Liang, X., Guo, S., Huang, C., Wang, B., Xiao, Y., He, J.,…Guan, Q. (2024). Modeling the Subpixel Land-Use Dynamics and Its Influence on Urban Heat Islands: Impacts of Factors and Scale, and Population Exposure Risk. *Sustainable Cities and Society*, *107*, 105417. doi:10.1016/j.scs.2024.105417.

Liu, X., Liang, X., Li, X., Xu, X., Ou, J., Chen, Y.,…Pei, F. (2017). A future land use simulation model (FLUS) for simulating multiple land use scenarios by coupling human and natural effects. *Landscape and Urban Planning*, *168*, 94-116. doi:10.1016/j.landurbplan.2017.09.019.

Masoudi, M., Tan, P. Y., & Fadaei, M. (2021). The effects of land use on spatial pattern of urban green spaces and their cooling ability. *Urban Climate, 35*, Article 100743. https://doi.org/10.1016/j.uclim.2020.100743

Meimei, W., Zizhen, J., Tengbiao, L., Yongchun, Y., & Zhuo, J. (2023). Analysis on absolute conflict and relative conflict of land use in Xining metropolitan area under different scenarios in 2030 by PLUS and PFCI. *Cities*, *137*, 104314. doi:10.1016/j.cities.2023.104314.

O'Malley, C., & Kikumoto, H. (2022). An investigation into heat storage by adopting local climate zones and nocturnal-diurnal urban heat island differences in the Tokyo Prefecture. *Sustainable Cities and Society, 83*, Article 103959. https://doi.org/10.1016/j.scs.2022.103959

O'Malley, C., & Kikumoto, H. (2021). An investigation into the relationship between remotely sensed land surface temperatures and heat stroke incident rates in the Tokyo Prefecture 2010–2019. *Sustainable Cities and Society, 71*, Article 102988. https://doi.org/10.1016/j.scs.2021.102988

O'Neill, B. C., Kriegler, E., Riahi, K., Ebi, K. L., Hallegatte, S., Carter, T. R.,…van Vuuren, D. P. (2014). A new scenario framework for climate change research: the concept of shared socioeconomic pathways. *Climatic Change*, *122*(3), 387-400. doi: 10.1007/s10584-013-0905-2.

Pan, T., Su, F., Yan, F., Lyne, V., Wang, Z., & Xu, L. (2023). Optimization of multi-objective multi-functional landuse zoning using a vector-based genetic algorithm. *Cities*, *137*, 104256. doi:10.1016/j.cities.2023.104256.

Pan, T., Zhang, Y., Su, F., Lyne, V., Cheng, F., & Xiao, H. (2021). Practical efficient regional land-use planning using constrained multi-objective genetic algorithm optimization. *ISPRS International Journal of Geo-Information, 10*(2).

Parsaee, M., Joybari, M. M., Mirzaei, P. A., & Haghighat, F. (2019). Urban heat island, urban climate maps and urban development policies and action plans. *Environmental Technology & Innovation, 14*, Article 100341. https://doi.org/10.1016/j.eti.2019.100341

Peng, H., Lou, H., Yang, Y., He, Q., Liu, Y., Chen, E., & Zhang, M. (2025). Spatial and temporal heterogeneity of human- air-ground coupling relationships at fine scale. *Polish Journal of Environmental Studies.*. https://doi.org/10.15244/pjoes/197055

Qiu, J., Li, X., & Qian, W. (2023). Optimizing the spatial pattern of the cold island to mitigate the urban heat island effect. *Ecological Indicators, 154*, Article 110550. https://doi.org/10.1016/j.ecolind.2023.110550

Rahman, M. M., & Szabó, G. (2021). Multi-objective urban land use optimization using spatial data: A systematic review. *Sustainable Cities and Society, 74*, Article 103214. https://doi.org/10.1016/j.scs.2021.103214

Santamouris, M. (2020). Recent progress on urban overheating and heat island research. Integrated assessment of the energy, environmental, vulnerability and health impact. Synergies with the global climate change. *Energy and Buildings, 207*, Article 109482. https://doi.org/10.1016/j.enbuild.2019.109482

Song, M., & Chen, D. (2018). A comparison of three heuristic optimization algorithms for solving the multi-objective land allocation (MOLA) problem. *Annals of GIS, 24*(1), 19–31. https://doi.org/10.1080/19475683.2018.1424736

Song, Y., Wang, J., Ge, Y., & Xu, C. (2020). An optimal parameters-based geographical detector model enhances geographic characteristics of explanatory variables for spatial heterogeneity analysis: Cases with different types of spatial data. *GIScience & Remote Sensing, 57*(5), 593–610. https://doi.org/10.1080/15481603.2020.1760434

Stewart, I. D., & Oke, T. R. (2012). Local climate zones for urban temperature studies. *Bulletin of the American Meteorological Society, 93*(12), 1879–1900. https://doi.org/10.1175/BAMS-D-11-00019.1

Tan, X., Sun, X., Huang, C., Yuan, Y., & Hou, D. (2021). Comparison of cooling effect between green space and water body. *Sustainable Cities and Society, 67*, Article 102711. https://doi.org/10.1016/j.scs.2021.102711

Tanoori, G., Soltani, A., & Modiri, A. (2024). Machine learning for urban heat island (UHI) analysis: predicting land surface temperature (LST) in urban environments. *Urban Climate, 55*, Article 101962. https://doi.org/10.1016/j.uclim.2024.101962

Tong, Z., Liu, Y., Zhang, Z., Pang, B., An, R., Lu, Y.,…Wang, H. (2024). Incorporating historical information into the multi-type ant colony optimization model to optimize patch-level land use allocation. *Sustainable Cities and Society*, *106*, 105404. doi:10.1016/j.scs.2024.105404.

Tong, Z., Yang, J., Liu, Y., Zhang, Z., Liu, S., Lu, Y.,…An, R. (2024). Cooling and optimizing urban heat island based on a thermal knowledge-informed multi-type ant colony model. *Remote Sensing of Environment*, *306*, 114138. doi:10.1016/j.rse.2024.114138.

Vanderhaegen, S., & Canters, F. (2017). Mapping urban form and function at city block level using spatial metrics. *Landscape and Urban Planning, 167*, 399–409. https://doi.org/10.1016/j.landurbplan.2017.05.023

Varentsova, S. A., & Varentsov, M. I. (2021). A new approach to study the long-term urban heat island evolution using time-dependent spectroscopy. *Urban Climate, 40*, Article 101026. https://doi.org/10.1016/j.uclim.2021.101026

Verburg, P. H., Tabeau, A., & Hatna, E. (2013). Assessing spatial uncertainties of land allocation using a scenario approach and sensitivity analysis: A study for land use in Europe. *Journal of Environmental Management, 127*, S132–S144. https://doi.org/10.1016/j.jenvman.2012.08.038

Wang, A., Dai, Y., Zhang, M., & Chen, E. (2025). Exploring the cooling intensity of green cover on urban heat island: A case study of nine main urban districts in Chongqing. *Sustainable Cities and Society, 124*, Article 106299. https://doi.org/10.1016/j.scs.2025.106299

Wang, A., Wang, J., Zhang, R., & Cao, S.-J. (2024). Mitigating urban heat and air pollution considering green and transportation infrastructure. *Transportation Research Part A: Policy and Practice, 184*, Article 104079. https://doi.org/10.1016/j.tra.2024.104079

Wang, C., Wei, S., Du, S., Zhuang, D., Li, Y., Shi, X.,…Zhou, X. (2021). A systematic method to develop three dimensional geometry models of buildings for urban building energy modeling. *Sustainable Cities and Society*, *71*, 102998. doi:10.1016/j.scs.2021.102998.

Wang, D., Tan, D., & Liu, L. (2018). Particle swarm optimization algorithm: An overview. *Soft Computing, 22*(2), 387–408. https://doi.org/10.1007/s00500-016-2474-6

Wang, N., Yue, Z., Tong, Z., Liu, Y., & Liu, Y. (2024). A multi-objective optimization framework for regional land-use allocation: Fully utilizing terrestrial vegetation to mitigate carbon emissions. *Journal of Cleaner Production, 479*, Article 144058. https://doi.org/10.1016/j.jclepro.2024.144058

Wang, R., Wang, M., Ren, C., Chen, G., Mills, G., & Ching, J. (2024). Mapping local climate zones and its applications at the global scale: A systematic review of the last decade of progress and trend. *Urban Climate, 57*, Article 102129. https://doi.org/10.1016/j.uclim.2024.102129

Wang, Z., Peng, Y., Li, Y., Zhou, X., & Xie, Y. (2024). Exploration of influencing factors of land surface temperature in cities within the beijing–Tianjin–Hebei region based on local climate zone scheme. *IEEE Journal of Selected Topics in Applied Earth Observations and Remote Sensing, 17*, 9728–9744. https://doi.org/10.1109/JSTARS.2024.3396167

Wardeh, Y., Kinab, E., Escadeillas, G., Rahme, P., & Ginestet, S. (2022). Review of the optimization techniques for cool pavements solutions to mitigate Urban Heat Islands. *Building and Environment, 223*, Article 109482. https://doi.org/10.1016/j.buildenv.2022.109482

Wu, J. (2014). Urban ecology and sustainability: The state-of-the-science and future directions. *Landscape and Urban Planning, 125*, 209–221. https://doi.org/10.1016/j.landurbplan.2014.01.018

Wu, W.-B., Yu, Z.-W., Ma, J., & Zhao, B. (2022). Quantifying the influence of 2D and 3D urban morphology on the thermal environment across climatic zones. *Landscape and Urban Planning, 226*, Article 104499. https://doi.org/10.1016/j.landurbplan.2022.104499

Xu, X., Ou, J., Liu, P., Liu, X., & Zhang, H. (2021). Investigating the impacts of three-dimensional spatial structures on CO2 emissions at the urban scale. *Science of The Total Environment, 762*, Article 143096. https://doi.org/10.1016/j.scitotenv.2020.143096

Yang, K., Zhang, J., Cui, D., Ma, Y., Ye, Y., He, X.,…Zhang, Y. (2025). Multi-scale study of the synergy between human activities and climate change on urban heat islands in China. *Sustainable Cities and Society*, *125*, 106341. doi:10.1016/j.scs.2025.106341.

Yang, X., & Li, Y. (2015). The impact of building density and building height heterogeneity on average urban albedo and street surface temperature. *Building and Environment, 90*, 146–156. https://doi.org/10.1016/j.buildenv.2015.03.037

Yao, Y., Liu, X., Li, X., Liu, P., Hong, Y., Zhang, Y., & Mai, K. (2017). Simulating urban land-use changes at a large scale by integrating dynamic land parcel subdivision and vector-based cellular automata. *International Journal of Geographical Information Science, 31*(12), 2452–2479. https://doi.org/10.1080/13658816.2017.1360494

Yu, X., Liu, Y., Zhang, Z., & Xiao, R. (2021). Influences of buildings on urban heat island based on 3D landscape metrics: An investigation of China's 30 megacities at micro grid-cell scale and macro city scale. *Landscape Ecology, 36*(9), 2743–2762. https://doi.org/10.1007/s10980-021-01275-x

Yu, Z., Guo, X., Jørgensen, G., & Vejre, H. (2017). How can urban green spaces be planned for climate adaptation in subtropical cities? *Ecological Indicators, 82*, 152–162. https://doi.org/10.1016/j.ecolind.2017.07.002

Zhang, H., Li, T.-T., & Han, J.-J. (2020). Quantifying the relationship between land use features and intra-surface urban heat island effect. Study on downtown Shanghai. *Applied Geography, 125*, Article 102305. https://doi.org/10.1016/j.apgeog.2020.102305

Zhang, J., Li, Z., & Hu, D. (2022). Effects of urban morphology on thermal comfort at the micro-scale. *Sustainable Cities and Society, 86*, Article 104150. https://doi.org/10.1016/j.scs.2022.104150

Zhang, M., Yiğit, İ., Adigüzel, F., Hu, C., Chen, E., Siyavuş, A. E.,…Kaya, A. Y. (2024). Impact of Urban Surfaces on Microclimatic Conditions and Thermal Comfort in Burdur, Türkiye. *Atmosphere*, *15*(11).

Zhao, X., He, J., Luo, Y., & Li, Y. (2022). An analytical method to determine typical residential district models for predicting the urban heat island effect in residential areas. *Urban Climate, 41*, Article 101007. https://doi.org/10.1016/j.uclim.2021.101007

Zhou, W., Pickett, S. T. A., & Cadenasso, M. L. (2017). Shifting concepts of urban spatial heterogeneity and their implications for sustainability. *Landscape Ecology, 32*(1), 15–30. https://doi.org/10.1007/s10980-016-0432-4

Zhou, X., & Chen, H. (2018). Impact of urbanization-related land use land cover changes and urban morphology changes on the urban heat island phenomenon. *Science of The Total Environment, 635*, 1467–1476. https://doi.org/10.1016/j.scitotenv.2018.04.091

Zhu, Z., Shen, Y., Fu, W., Zheng, D., Huang, P., Li, J.,…Yao, X. (2023). How does 2D and 3D of urban morphology affect the seasonal land surface temperature in Island City?

A block-scale perspective. *Ecological Indicators*, *150*, 110221. doi:10.1016/j.ecolind.2023.110221.